AeoLiS

Numerical modelling of coastal dunes and aeolian landform development for real-world applications

van Westen, Bart; de Vries, Sierd; Cohn, Nicholas; van IJzendoorn, Christa; Strypsteen, Glenn; Hallin, Caroline

Important note
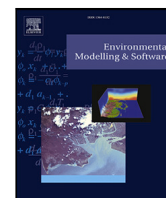To cite this publication, please use the final published version (if applicable).
Please check the document version above.

Position Paper

AeoLiS: Numerical modelling of coastal dunes and aeolian landform development for real-world applications

Bart van Westen [a,b,*,1], Sierd de Vries [b,1], Nicholas Cohn [c], Christa van IJzendoorn [b,d], Glenn Strypsteen [e], Caroline Hallin [b,f]

[a] *Deltares, Boussinesqweg 1, Delft, 2629 HV, Netherlands*
[b] *Delft University of Technology, Department of Civil Engineering and Geosciences, Stevinweg 1, Delft, 2628 CN, Netherlands*
[c] *U.S. Army Engineer Research and Development Center, Coastal and Hydraulics Laboratory, 1261 Duck Road, Duck, NC, 27949, USA*
[d] *Oregon State University, College of Earth, Ocean, and Atmospheric Sciences, 101 SW 26th St., Corvallis, OR, 97331, USA*
[e] *Hydraulics and Geotechnics, Department of Civil Engineering, Bruges Campus, KU Leuven, Spoorwegstraat 12, Bruges, 8200, Belgium*
[f] *Lund University, Division of Water Resources Engineering, John Ericssons Väg 1, Lund, Sweden*

ARTICLE INFO

ABSTRACT

The formation and evolution of coastal dunes result from a complex interplay of eco-morphodynamic processes. State-of-the-art models can simulate aeolian transports and morphological dune evolution under certain conditions. However, a model combining these processes for coastal engineering applications was not yet available. This study aims to develop a predictive tool for dune development to inform coastal management decisions and interventions. The aeolian sediment transport model AeoLiS is extended with functionalities that allow for simulations of coastal landforms. The added functionalities include the effect of topographic steering on wind shear, avalanching of steep slopes and vegetation processes in the form of growth and wind shear reduction. The model is validated by simulating four distinct coastal landforms; barchan-, parabolic-, embryo dunes and blowouts. Simulations, based on real-world conditions, replicate the landform formation, migration rates and seasonal variability.

1. Introduction

Coastal dunes display a variety of shapes, sizes and behaviours that support numerous ecosystem services. Such ecosystem services include enhancing flood protection, increasing natural and recreational value, and reducing sand nuisance on adjoining infrastructure (van der Meulen and de Haes, 1996; Everard et al., 2010; Barbier et al., 2011; Borsje et al., 2011; Biel et al., 2017; van der Biest et al., 2017; Strypsteen et al., 2024). At some locations, primarily in the Netherlands, coastal dunes also assist in the provision of drinking water (Bakker and Stuyfzand, 1993; Geelen et al., 2017). The dynamic eco-morphological development of coastal dunes results in different characteristic landforms, such as linear foredune ridges, hummocky dunes, parabolic dunes, and blowouts (Hesp, 2002). Dunes in the coastal zone naturally evolve in response to a combination of aeolian processes (e.g., wind energy and sediment supply), biotic processes (e.g., growth of plant communities), and marine processes (e.g., wave energy, tide and littoral drift direction) (Pye, 1983; Short and Hesp, 1982; Hesp, 2002; Martínez and Psuty, 2004; Hesp and Smyth, 2016; Cohn et al., 2018; Brodie et al.,

2019), as well as, active and passive anthropogenic influences (Nordstrom et al., 2000; Jackson and Nordstrom, 2011; Provoost et al., 2011; Martínez et al., 2013; Delgado-Fernandez et al., 2019; Wijnberg et al., 2021).

Management of coastal dunes is increasingly applied to optimize different ecosystem services. The flood protection service is typically enhanced through nourishments and the planting of *Ammophila arenaria* (marram grass) to stabilize, restore or promote the generation of (new) coastal dunes (Ranwell and Rosalind, 1986; van der Wal, 2004; Matias et al., 2005; Bakker et al., 2012; Stive et al., 2013; Sigren et al., 2014; Hoonhout and de Vries, 2017; Wittebrood et al., 2018; de Schipper et al., 2021; Derijckere et al., 2022; Kroon et al., 2022; Brand et al., 2022; Derijckere et al., 2023; Walker et al., 2023; Strypsteen et al., 2024; van Westen et al., 2024). In contrast, biodiversity may be promoted by the removal of vegetation and sediment by excavating notches in the foredune. Removing vegetation and sediment may promote sediment transport beyond the foredune towards the hinterland, and facilitate landward dune migration in response to sea

---

Fig. 1. Three dune intervention projects, having varying objectives. (a) Five notches in the foredune at the National Park Zuid-Kennemerland (NPZK) purposefully excavated to reintroduce dune dynamics. (b) The 21 Mm³ Sand Engine mega nourishment, constructed to stimulate dune development. (c) An artificial dune constructed in front of an existing seawall as part of the Dune-in-front-of-Dike project to limit sand nuisance.

level rise (van Boxel et al., 1997; Arens et al., 2013; Walker et al., 2013; Ruessink et al., 2018; Castelle et al., 2019). The photos in Fig. 1 show three specific examples of active dune interventions; (i) excavated foredune notches at Dutch National Park Zuid-Kennemerland promoting dune dynamics (Ruessink et al., 2018); (ii) the Sand Engine mega nourishment designed to feed the adjacent coast and stimulate dune development (Stive et al., 2013); (iii) an artificially constructed dune along the Belgium coast to mitigate sand nuisance (Derijckere et al., 2022, 2023; Strypsteen et al., 2024). Although some coastal communities share positive experiences as a result of dune management, debates exist about the general usefulness of measures to optimize ecosystem services (Delgado-Fernandez et al., 2019; Arens et al., 2020). Dune management has even been critically labelled as *dune gardening* by some (Cooper and Jackson, 2021). At the same time, uncertainties with respect to the foreseen benefits of dune management measures remain.

To reduce uncertainties about the impact of dune management measures, numerical modelling tools may assist in describing and predicting the future development of coastal dunes. To be able to inform the design of dune management interventions, a numerical tool should involve accurate, quantitative and reliable descriptions of the *processes governing dune development* (Section 2.1) and thus, be capable of simulating typical *coastal dune landforms* (Section 2.2). In recent years some notable *state-of-the-art dune models* (Section 2.3) have been proposed that may inspire a new comprehensive approach and provide a starting point.

Recognizing some of the deficiencies in current open-source tools for simulating the range of relevant eco-morphodynamic processes that drive coastal dune evolution for engineering timescales (days to decades), the objective of this study is to present an improved model to simulate the development of dunes in coastal areas that is applicable in practical situations. In the paper, the model's capabilities are demonstrated by simulating four distinct aeolian dune landforms (see Fig. 2) and validating the outcomes with available data. Background information regarding processes governing dune development, typical coastal dune landforms and state-of-the-art dune models is given in Section 2. Section 3 presents new formulations added to the AeoLiS model (Hoonhout and de Vries, 2016) to achieve these applied objectives. Section 4 presents the model setup and validation approach for these four demonstration cases and Section 5 presents results for these select cases. A discussion and conclusions are provided in Sections 6 and 7, respectively.

2. Coastal dune processes, landforms, and models

2.1. Processes governing landform development

Wind-driven sediment transport is the main driver of dune growth. The majority of available methods to predict aeolian sediment transport rates are based on the pioneering work by Bagnold (1937). Bagnold (1937) describes that the magnitude of aeolian sediment transport is dependent on a 3rd power of the wind velocity. However, in coastal environments, supply-limitations are believed to reduce aeolian transport to below the potential wind-driven transport capacity (Davidson-Arnott and Law, 1996; de Vries et al., 2014). Many factors that can limit sediment supply have been described in literature. Examples of supply-limiting conditions are soil moisture (Bauer et al., 2009; Ruessink et al., 2022; Hallin et al., 2023a), and sediment sorting leading to the formation of desert pavements and armouring of the sediment surface (Carter, 1976; van IJzendoorn et al., 2023; Hoonhout and de Vries, 2017; Uphues et al., 2022; Strypsteen and Rauwoens, 2023).

Wind shear varies spatially due to the interaction between coastal topography and wind flow. Horizontal wind flows may converge and diverge vertically when travelling up and downhill respectively. Converging and diverging wind flows lead to respective acceleration and deceleration of flow. Topographic features (steep gradients and/or structures) can also disrupt the flow, causing separation and even reversal of flow (Walker and Nickling, 2002; Bauer et al., 2012; Hesp et al., 2015; Strypsteen et al., 2020). The topographic steering of wind in coastal environments can shape coastal dune and beach morphology by influencing the location of sediment erosion and deposition (Arens, 1996). As a result, the topographic steering of wind can play a significant role in maximizing the heights of foredunes (Durán and Moore, 2013), stimulating blowout formation (Hesp, 2002; Ruessink et al., 2018; van Kuik et al., 2022), and modulating wind shear stresses across the beachface (Bauer, 1991).

Vegetation plays a key role in the development of dunes (Bonte et al., 2021). The presence of vegetation reduces the wind shear near the bed which may cause a spatial gradient in sediment transport and local depositions of sediments (Raupach et al., 1993; Durán and Herrmann, 2006; Keijsers et al., 2015). Dune vegetation species, such as marram grass, are characterized by their sand-trapping ability and capacity to grow with significant burial. The growth of some vegetation species may even be enhanced for certain sediment burial rates (Baas and Nield, 2007; Maun, 2009; Keijsers et al., 2016; Nolet et al., 2018). In addition to sediment burial rates, the establishment, growth, and resilience of dune vegetation are governed by numerous biotic and abiotic conditions, such as salinity, acting wind stress, groundwater levels, competition and removal by storm erosion (Maun, 2009; van Puijenbroek et al., 2017b; Homberger et al., 2024).

In coastal areas, the development of coastal dunes is influenced by marine dynamics (Cohn et al., 2018; van Westen et al., 2024) in addition to aeolian processes. The waterline provides a boundary condition to the aeolian domain and the exchange of sediment across the waterline (or intertidal zone) is governed by both marine and aeolian activities (Short and Hesp, 1982; Houser, 2009). Wave actions may influence the sediment availability for aeolian transport (Bauer et al., 2009; de Vries et al., 2014; Hallin et al., 2023a). Also, extreme weather events can kill or remove vegetation causing erosion of the dunes. The combination of marine and aeolian processes contribute to the formation of coastal dunes.
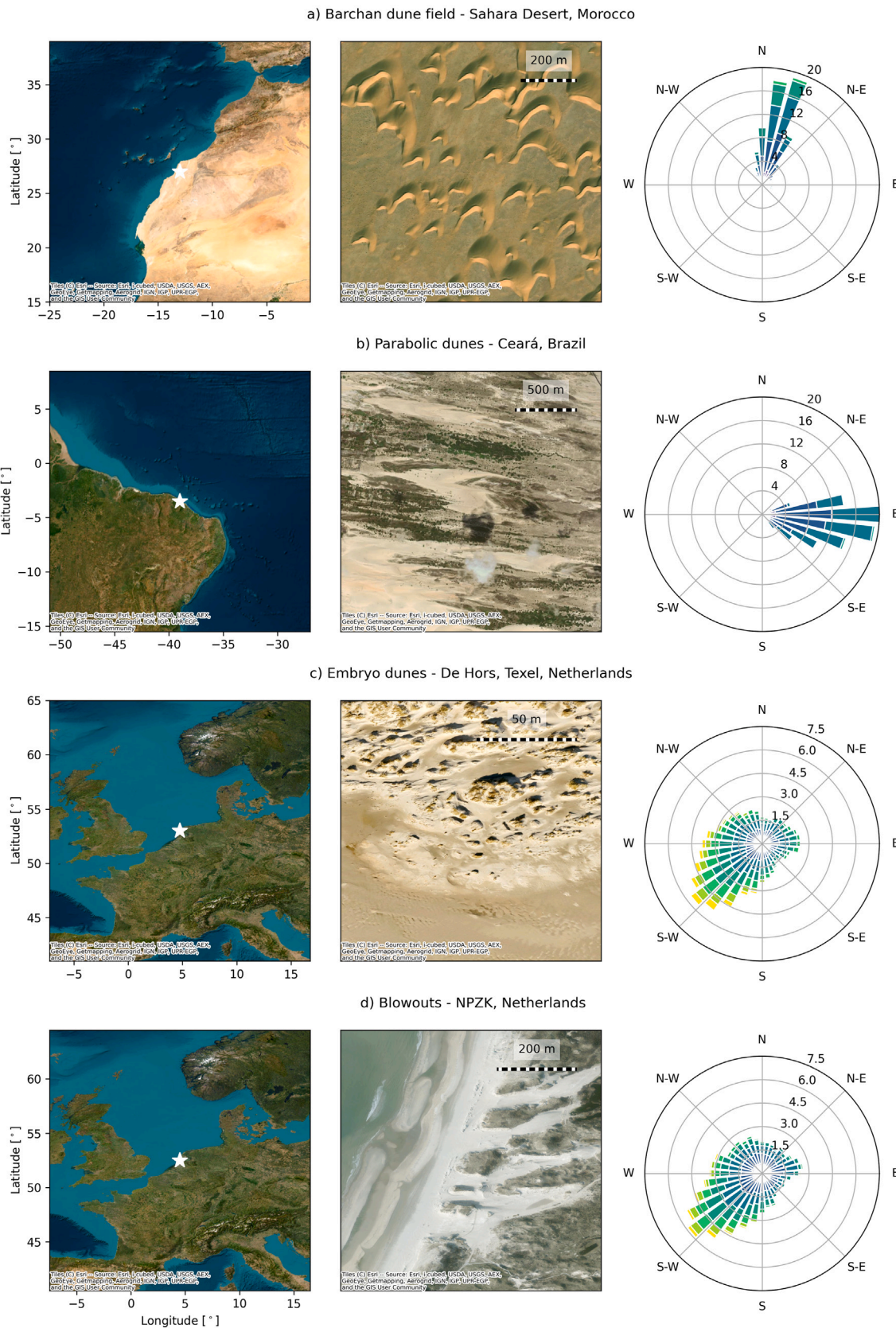
Fig. 2. An overview of real-world cases of four aeolian landforms central in this study: (a) barchan dunes, (b) parabolic dunes, (c) embryo dunes, and (d) artificial blowouts. The centre panels show a satellite view of each landform. The selected locations are shown in the left panels, and the wind forcing in the right panels, which are based on the ERA5 hindcast.

2.2. Aeolian landforms and coastal dunes

Aeolian landforms are shaped by a complex interplay of the governing processes. In this study, four distinct types of aeolian landforms, having unique characteristics in terms of dimensions and dynamics, are used as demonstration cases. Real-world examples, as shown in Fig. 2 are used for the setup and validation of the model (Section 3).

Barchan dunes (Fig. 2a) are crescent-shaped and migrate windward under relatively uniform wind conditions, which are characteristic of desert environments with limited sediment supply (Hesp and Hastings, 1998; Sauermann et al., 2000; Hersen et al., 2002; Hersen, 2004). Several measurements have been carried out to measure the morphological shape, size, and migration velocity (Hesp and Hastings, 1998; Sauermann et al., 2000; Hamdan et al., 2016, e.g.). Barchan dunes have previously been used in modelling studies due to their typical and measurable shape and the simple conditions under which barchan dunes develop (Hersen, 2004; Parteli et al., 2007; Durán et al., 2010; Zhang et al., 2010; Parteli et al., 2014).

Parabolic dunes (Fig. 2b) are vegetated dunes that migrate along the prevailing wind direction (Durán et al., 2008). The growth of vegetation can cause crescent dunes to be fixated and transformed into parabolic dunes, as addressed by several observations and modelling applications (Barchyn and Hugenholtz, 2012; Reitz et al., 2010; Anthonsen et al., 1996; Baas and Nield, 2007; Durán and Herrmann, 2006). Regions with relatively large sediment transports stay morphologically active and are often covered by vegetation, as erosion is strong enough to prevent growth. At the trailing horns, the stabilizing effect of vegetation is dominant, resulting in a U-shaped landform with its nose pointing downwind as opposed to the barchan dunes. In models that describe the formation of a parabolic dune, the magnitude of the active sediment transport must be in balance with the stabilizing effects of vegetation. Parabolic dunes make an ideal demonstration case for the impact of vegetation on sedimentation and erosion patterns and, thus, the long-term morphodynamic landform development.

Embryo dunes (Fig. 2c), alternatively referred to as incipient or Nebkha dunes, are the first stage of development of coastal dunes (Hesp, 1989, 2002; Nield and Baas, 2008; van Puijenbroek et al., 2017a; Hesp and Smyth, 2017; Bonte et al., 2021). After establishment, initial vegetation grows vertically and laterally, causing an embryo dune to grow. The formation of several embryo dunes may occur in parallel over a large space, and embryo dunes of similar shape and size can often be found in fields. Embryo dunes and accompanying vegetation may be washed away when they are submerged during high-water events. Embryo dunes may, therefore, often be a temporary or intermittent feature. However, embryo dunes can also grow to become established coastal foredunes (Montreuil et al., 2013).

Blowouts (Fig. 2d) are erosional features that form depressions within coastal dune systems (Hesp, 2002). Blowout initiation primarily occurs through the action of wind erosion, often at locations where the vegetation cover is weakened due to natural or anthropogenic impact, such as trampling (Schwarz et al., 2018). The wind erosion enlarges and deepens these initial depressions, creating the distinct bowl-shaped or elongated structures characteristic of blowouts. Vegetation growth on the trailing arms can transform the blowout into a parabolic-shaped landform (Hesp, 2002; Arens et al., 2013; van Kuik et al., 2022; Laporte-Fauret et al., 2022). The closure of blowouts is driven by the re-establishment of vegetation at the blowout entrance, partially stabilizing the surface and preventing further erosion (Schwarz et al., 2018). In recent years, artificial blowouts created through vegetation removal or sand excavation have been implemented for nature conservation purposes (Fig. 1).

2.3. Aeolian transport and dune models

In recent decades, development has shifted from qualitative descriptions of coastal dune development (Short and Hesp, 1982; Hesp, 2002) to more quantitatively predictive tools (de Vries et al., 2014; Durán and Moore, 2013; Keijsers et al., 2016; Roelvink and Costas, 2019). We give an overview of several numerical models for coastal dune development that have been presented in recent years.

DUne BEach VEGetation (Keijsers et al., 2016; Wijnberg et al., 2021, DUBEVEG) is a cellular automaton simulating long-term growth of extensive dune systems using probabilistic rules for erosion, deposition, and vegetation dynamics. DUBEVEG includes vegetation growth as a function of sedimentation, destruction due to seawater, lateral propagation, and establishment.

The *Coastal Dune Model* (Durán and Moore, 2013, CDM) depicts the morphodynamic evolution of vegetated coastal foredunes. CDM can simulate rates of aeolian sediment transport and the eco-morphological feedback with topography and vegetation. It can produce complex shapes that rely on morphological feedbacks like parabolic and barchan dunes. However, it does not account for supply limitations affecting sediment availability for transport, and the wind conditions are implemented only for winds directly perpendicular to the shoreline.

DUNA (Roelvink and Costas, 2019) is a 1D dune profile model, particularly developed as an aeolian extension to the XBeach model (Roelvink et al., 2009). This coupling to the XBeach model allows for marine–aeolian interactions. Similarly to CDM, DUNA is based on a process-based description of aeolian sediment transport, in combination with topographic feedback and the shear-reducing effect of vegetation. Supply limitations are included through a parameterized approach, which may improve quantitative predictions. The current one-dimensional setup limits its applicability to coastal profiles only.

Psamathe (Ruessink et al., 2022) is a model that focuses on predicting aeolian sediment transport rates and the associated growth of foredunes on narrow beaches over periods ranging from months to several years. The model uses a fetch based approach to account for sediment supply limitations. It integrates the processes related to a spatially and temporally varying groundwater table, surface moisture content and aeolian sand transport rate on a sandy beach.

AeoLiS is a process-based model simulating aeolian sediment transport under supply-limited conditions. It is based on one-dimensional process descriptions by de Vries et al. (2014), Hoonhout and de Vries (2016). Hoonhout and de Vries (2019) extended the model to be applicable to two-dimensional spatial domains that are relevant to specific management situations. Up until the current work it mainly describes multi-fractional sediment transport and various controls on sediment availability in both one and two spatial dimensions (van IJzendoorn et al., 2023; Hallin et al., 2023a). At the start of this study, it did not encompass morphological feedback and dune-building processes like topographic steering and vegetation dynamics.

State-of-the-art numerical tools that describe sediment transport and dune development have provided valuable insights. However, the usability of these individual models remains limited for management applications because the processes, spatiotemporal resolutions and timescales between models and applications do not match. Either not all relevant processes are sufficiently included, or the applicability of the model is restricted by practical limitations (e.g., one-dimensional profile model or only perpendicular winds).

For this study, we use the AeoLiS sediment transport model as a starting point, given its open-source availability and modular setup. We extend the AeoLiS sediment transport model using new process implementations of essential processes that describe dune development. Concepts of existing models like CDM and DUBEVEG serve as inspiration for part of this work and we provide references to the original work where appropriate.
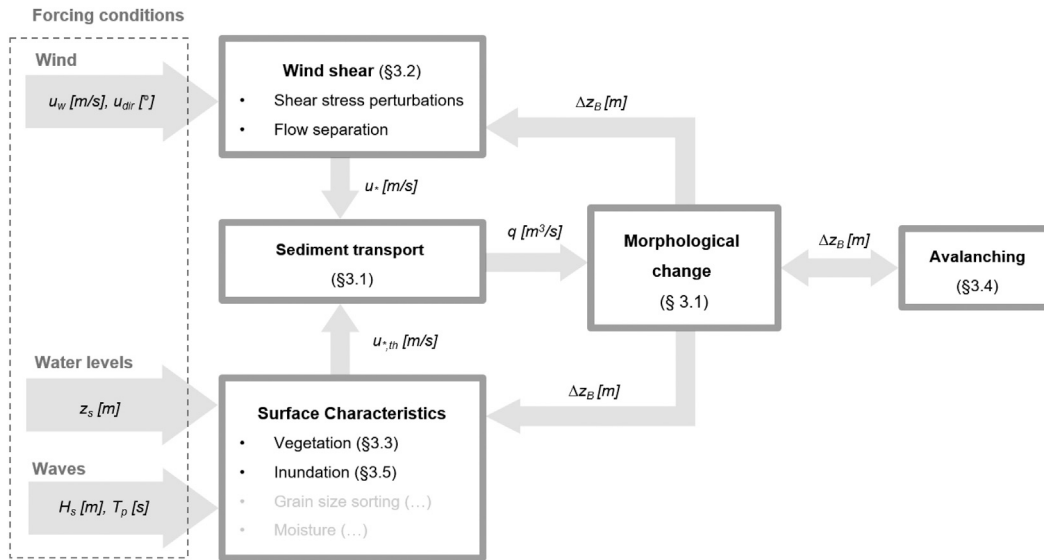
Fig. 3. Flowchart showing the implemented processes in AeoLiS.

3. Model implementations of processes

AeoLiS is extended here with functionalities relative to the original open-source model as presented by Hoonhout and de Vries (2016) that allow for the simulation of landforms by implementing the effect of topographic steering on wind shear, vegetation processes in the form of vertical growth, lateral spreading, and reduced wind shear, as well as avalanching of steep slopes and swash impact on vegetation and dune formation. For comprehensive details on the pre-existing core functionalities of the AeoLiS model readers are directed to de Vries et al. (2014), Hoonhout and de Vries (2016) and van IJzendoorn et al. (2023). For the landform development described in this paper, the moisture module (Hallin et al., 2023a) and grain size sorting module (van IJzendoorn et al., 2023) are not used. The model structure and the relation between all implemented processes are illustrated in Fig. 3.

The forcing conditions of AeoLiS consist of wind speed, wind direction, water levels and wave conditions. All forcing conditions can be assumed constant but may also vary in time. Although not applied in this study, it is technically also feasible to input spatially variable forcings into the model.

3.1. Sediment transport and morphological change

AeoLiS involves a two-dimensional continuum approach to sediment transport including sedimentation and erosion in Eulerian space. This is described after Hoonhout and de Vries (2019) as:

$$\frac{\partial c}{\partial t} + u_{\text{sed,x}} \frac{\partial c}{\partial x} + u_{\text{sed,y}} \frac{\partial c}{\partial y} = E - D \tag{1}$$

where c [kg/m^3] is the sediment concentration in the air. $u_{\text{sed,x}}$ [m/s] and $u_{\text{sed,y}}$ [m/s] are horizontal sediment velocities in x- and y-direction respectively. The right-hand side of Eq. (1) describes the exchange of sediment with the bed where D [kg/m^2/s] represents potential deposition and E [kg/m^2/s] the potential erosion. Erosion and deposition is governed by the concentration at transport saturation c_{sat} [kg/m^3] and available sediment at the bed m_{a} [kg/m^2] through:

$$E - D = \min \left(\frac{\partial m_{\text{a}}}{\partial t} \quad ; \quad \frac{c_{\text{sat}} - c}{T} \right) \tag{2}$$

where T [s] is a timescale for sediment exchange between the sediment bed and the transport layer in the air. For the details on calculating saturated sediment transports and the potential erosion and deposition,

we refer to the work in de Vries et al. (2014), Hoonhout and de Vries (2016).

For simplicity, the horizontal sediment velocity u_{sed} may be assumed to be equal to the wind velocity u_w [m/s]. But, predictions of the actual saltation velocity could provide a more realistic description of the horizontal sediment velocity (Sauermann et al., 2001). The horizontal sediment velocity can be determined from the momentum balance that is described in Durán (2007) by three terms. Term I: the drag force acting on the grains. Term II: the loss of momentum when they splash on the ground. Term III: the downhill gravity force:

$$\frac{(\vec{v_{eff}} - \vec{u_{sed}})|\vec{v_{eff}} - \vec{u_{sed}}|}{u_f^2} - \frac{\vec{u_{sed}}}{2\alpha|\vec{u_{sed}}|} - \nabla\vec{z}_B = 0 \tag{3}$$

where v_{eff} [m/s] is the effective wind velocity driving the grains, resulting from the feedback effect of sand transport within the saltation layer, being a function of the shear velocity u_* [m/s] and shear velocity threshold $u_{*,th}$ [m/s]. Furthermore, u_f [m/s] is the grain settling velocity and ∇z_B [−] is the downhill gravity force. The parameter α (= 0.42 [−] for d = 250 μm), acts as an effective restitution coefficient for the grainbed interaction. Note that the computed u_{sed} represents the collective horizontal sediment movement and not the velocity of individual grains. AeoLiS solves Eq. (3) iteratively for each timestep.

The update of bed levels z [m] is introduced as a function of erosion and deposition, varying over time:

$$\frac{\partial z}{\partial t} = \rho_{\text{sed}} \frac{1}{1-p} (E - D) \tag{4}$$

where ρ_{sed} [kg/m^3] is the sediment density and p [−] is the sediment porosity. (Note that Eqs. (1) and (4) are equivalent to the general Exner equation (Paola and Voller, 2005) when $\frac{\partial c}{\partial t} = 0$).

3.2. Wind shear and topographic steering

To simulate the topographic steering effects on desert and coastal landforms, numerous studies have utilized computational fluid dynamics (Wakes et al., 2010; Smyth et al., 2011; Hesp et al., 2015; Bauer and Wakes, 2022; Pourteimouri et al., 2023). However, the computational costs of these methods currently limit their use when long-term morphodynamic simulations tailored for engineering applications are pursued. To reduce computational costs, we adopt the techniques proposed by Durán and Moore (2013) that consist of an analytical approach tailored for calculating topographic wind steering for smooth topographies combined with a modelled separation bubble

mechanism. In addition to the adopted techniques by Durán and Moore (2013) we implemented the ability to use varying wind directions that occur in realistic situations.

The starting point for calculating near-bed shear velocity u_* [m/s] and topographic steering is the Prandtl–Von Karman's Law of the Wall. The Law of the wall is used to convert the wind velocity u_w [m/s] at height z [m] above the bed to the near-bed shear velocity:

$$u_* = \frac{u_w}{\ln \frac{z}{z_0}} \kappa \tag{5}$$

where z_0 [m] is the roughness height above the bed and κ [−] is the von Kármán constant for turbulent flow. z_0 can also be determined based on a roughness height predictor as described by van Rijn and Strypsteen (2020) and Strypsteen (2023).

The topographic steering of the wind due to smooth gradients is implemented following an analytical perturbation theory for turbulent boundary layer flow (Weng et al., 1991; Kroy et al., 2002). This method describes the topographic impact through perturbations in the shear stress τ [N/m^2] ($\tau = \rho_a u_*^2$):

$$\vec{\tau}(x, y) = \vec{\tau}_0 + |\vec{\tau}_0| \delta \vec{\tau}(x, y) \tag{6}$$

where $\delta \vec{\tau}(x, y)$ is the shear stress perturbation and τ_0 is the computed shear stress on a flat topography. For two-dimensional situations, the shear stress perturbation in x- and y-direction ($\delta \tau_x$ and $\delta \tau_y$) is computed in Fourier space. A more detailed description of the shear stress perturbation theory is given in Appendix A.

The implementation of the shear perturbation theory by Weng et al. (1991) is only valid in situations with relatively smooth surfaces. In coastal environments, the existence of slipfaces and vegetation often results in rougher terrain, featuring sharp edges and steep slopes which lead to separation of wind flow (Jackson et al., 2011; Davidson et al., 2022). The occurrence of such steep slopes limits the validity of the Weng et al. (1991) approach. To address this, a heuristic description of flow separation is used following CDM (Sauermann et al., 2001; Kroy et al., 2002; Durán and Moore, 2013). A smooth envelope is created, which separates the main flow when a sharp edge is detected in windward direction. This smooth envelope is called a separation bubble z_{sep} [m]. This separation bubble represents the surface that divides the region of flow reversal from the main flow stream along the smooth hill. Subsequently, in all cells for which the bed level is lower than the separation bubble ($z_B < z_{sep}$), the shear velocity u_* is set to 0 m/s. This assumes that eventual flow reversal velocities are not significant enough to initiate aeolian transport. The formulations describing the shape of the separation bubble are given in Appendix A.

The computed shear stress as a result of the combined influence of the implemented shear stress perturbations and flow separation is shown in Fig. 4. These results show the decrease on the windward- and lee-side of both Gaussian- and barchan-shaped landforms and an increase over the crest. Additionally, a shear velocity of zero is shown below the separation bubble. Studies have demonstrated the accuracy of the general analytical shear stress prediction approach applied to coastal dunes by comparing it with real-world measurements and detailed numerical simulation results acquired with CFD models (Computational Fluid Dynamics; Kombiadou et al., 2023; Cecil et al., 2024).

The implementation of the perturbation theory and separation bubble allows only for wind conditions that are perpendicular to the grid. To enable model applicability independent of wind direction, we developed a method that creates a secondary rotational grid that is aligned with the wind direction at each timestep, as shown in Video 1.

3.3. Vegetation at the sediment surface

Vegetation acts as a natural obstacle to aeolian sediment transport by reducing the near-bed shear stresses. The impact of vegetation on dune development is included in AeoLiS by describing the intrinsic development of vegetation, considering growth and decay due to burial (Durán and Moore, 2013), lateral growth and establishment (Keijsers et al., 2016), and the destruction of vegetation due to hydrodynamic processes is simulated by reducing vegetation density after cell inundation.

Durán and Moore (2013) describe the reduction of shear stress as a function of vegetation density (ρ_{veg}) and a dimensionless roughness factor (Γ).

$$\tau_s = \frac{\tau}{1 + \Gamma \rho_{veg}} \tag{7}$$

where τ_s is the remaining shear stress at the sediment surface. The default value of $\Gamma = 16$ is derived from vegetation geometry (Durán and Herrmann, 2006). The vegetation density ρ_{veg} varies in time and space as a function of vegetation growth and burial, and is assumed to be dependent on the maximum vegetation height $h_{veg,max}$ [m] and the vegetation height h_{veg} [m]:

$$\rho_{veg} = \left(\frac{h_{veg}}{h_{veg,max}} \right)^2. \tag{8}$$

where vegetation growth and decay are computed according to Durán and Herrmann (2006), reads:

$$\frac{\delta h_{veg}}{\delta t} = V_{ver} \left(1 - \frac{h_{veg}}{h_{veg,max}} \right) - \gamma_{veg} \left| \frac{\delta z_{b,veg}}{\delta t} \right| \tag{9}$$

with V_{ver} [m/s] representing the vertical growth rate of vegetation. The γ_{veg} [−] parameter is a sediment burial factor that accommodates the influence of sediment burial on vegetation growth.

The onset of vegetation may occur due to lateral propagation of vegetation or random establishment through germination. Once vegetation is established it is assumed to be able to grow and propagate laterally. The inherent uncertainties related to the random establishment of vegetation are implemented on a cell-by-cell basis by using a probabilistic approach, comparable to the cellular automata method discussed by Keijsers et al. (2016). AeoLiS accommodates assuming a germination probability ρ_{ger} [−] in every grid cell. This probability is assumed equal over the domain except for eroding grid cells (negative bed elevation change) where ρ_{ger} is assumed 0.

The onset of vegetation through lateral propagation per grid cell is derived by identifying the interfaces between vegetated and non-vegetated cells. The parameter ρ_{lat} alters the probability of lateral propagation at each interface.

3.4. Avalanching

Steep slopes may result from bed level changes that occur due to simulated sedimentation and erosion. The angle of repose θ_{ava} (default: 33°) determines the maximum slope that may exist due to the sediments' angle of internal friction. AeoLiS derives the spatial distribution of slopes based on each timestep's spatial gradients in morphology. If a critical slope is exceeded, a mass-conserving gravity-driven (downward) transport of sediment is simulated until all cells in the domain satisfy the critical slope. This technique is adopted from Durán and Moore (2013).

3.5. Marine influence

The sediment surface is submerged when the bed level is lower than the total water level (TWL). TWL is computed by adding the still water level and the computed run-up (Stockdon et al., 2006).
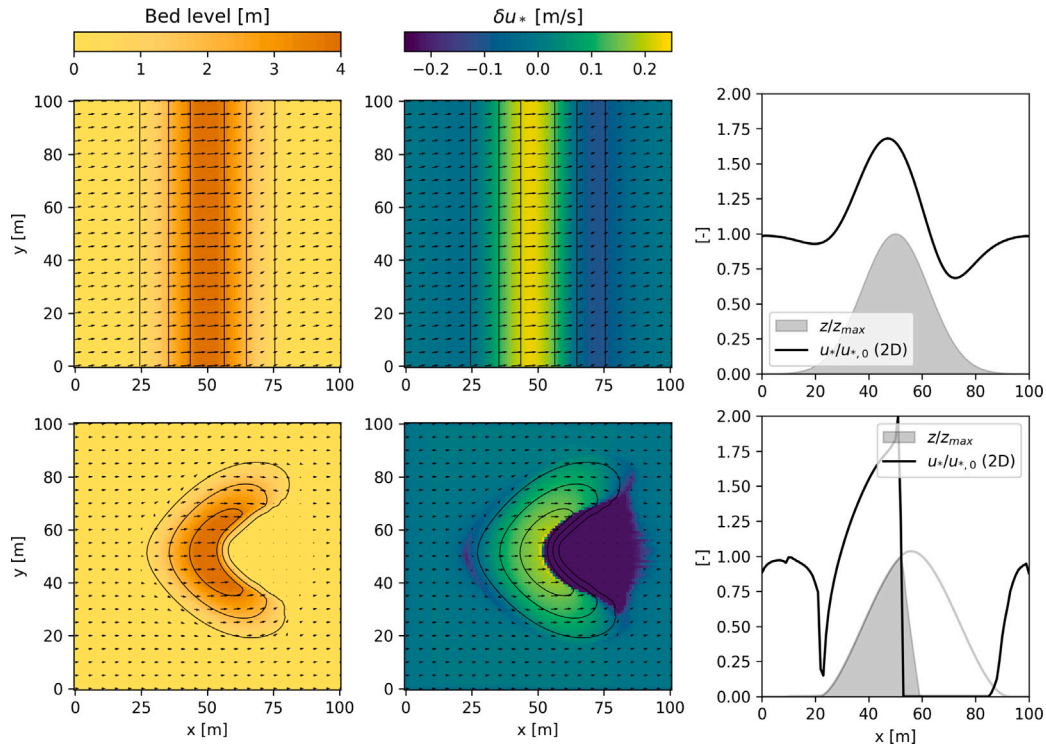
The model effects are threefold:

Fig. 4. Spatial variation in shear stress due to topographic steering of the wind field. The upper panels show the bed level z_B [m] and shear stress velocity perturbation δu_* [m/s] over a uniform Gaussian hill. The lower panels show topographic steering over a barchan dune, including the influence of flow separation. The right panels compare outcomes of the one- and two-dimensional approaches.

(i) Vegetation parameters are reset to zero, indicating the death of vegetation. This results in the intertidal zone or areas frequently inundated, typically lacking vegetation. Post-high water events, vegetation must re-establish in these areas;

(ii) The bed level slowly resets towards its initial position once submerged. Small dune features, such as embryo dunes, are levelled, and eroded sediment transport from the intertidal is re-supplied. This is based on the assumption that marine-driven morphodynamics dominate the intertidal.

(iii) The inundation of cells causes sand to be wet, reducing the aeolian sediment transport to 0 according to Hallin et al. (2023b).

4. Landform simulations

Simulations of four distinct landforms are used to illustrate the model's application range. The simulations are either subjected to academic conditions, to showcase key fundamental landform development, or real-world conditions to demonstrate the model's practical applicability at engineering scales. Wind data employed in the real-world simulations are derived from the ERA5 dataset (Hersbach et al., 2020), as illustrated in Fig. 2, except where specified otherwise. For consistency, all simulations are performed with one sediment fraction, assuming a diameter of 250 µm.

Both academic and real-world simulations are validated against existing literature and measurement data. Depending on the landform type and the availability of data, different characteristics are used for validation. Each landform-type simulation is connected to one of the landform-shaping processes. Barchan dunes are simulated to demonstrate the description of topographic steering. The influence of vegetation on sediment transport and vegetation establishment is demonstrated by simulating parabolic and embryo dunes, respectively. The development of real-world blowouts is simulated to demonstrate

all the processes above under real-world conditions, at an engineering scale.

A key aspect of the model setup is ensuring complete reproducibility of all simulations. Table B.1 provides a summary of these landform simulations, including the simulation names for reproduction.

4.1. Barchan dunes

A set of academic simulations is performed to verify the model's technical capacity to describe the characteristic crescentic shape of barchan dunes under varying wind conditions. Three mean wind directions are chosen (μ: 270, 45, 170 [°]). For each direction, different degrees of wind spreading are introduced (σ: 0, 22.5, 45 [°]), resulting in nine unique synthetic wind time series. The resulting crescentic shape should be independent of the wind direction, while the introduction of wind spreading is anticipated to yield a more rounded dune shape. Each series is generated by selecting 500 random wind events from a normal distribution based on each μ and σ pairing. The wind speed u_w is set at 12 m/s at a height of 10 m above the surface. The initial topography of each simulation is a cone-shaped feature in the centre of the computational domain with a volume of 13404 m^3, placed on top of a non-erodible layer ($z_{ne} = 0$ m).

For quantitative model validation, barchan dunes are simulated under real-world conditions in the Sahara desert, southern Morocco (see Fig. 2a). In 1999, Sauermann et al. (2000) measured various characteristic dimensions of eight barchan dunes. The wind conditions for the simulation are derived for the 1995–1999 period, preceding measurements by Sauermann et al. (2000). The initial topography replicates a cone-shaped feature, with the initial volume set to match the volumes by Sauermann et al. (2000). Circular boundary conditions are imposed to ensure mass conservation and a constant barchan dune volume over the simulation duration. The simulated period totals 24 years.

To validate the simulated barchan shape, the reported linear scalings between barchan dune volume, V [m^3], height, h [m], length, L [m] and width, W [m] are used (Hesp and Hastings, 1998; Sauermann et al., 2000). While the migration velocity was not directly measured by Sauermann et al. (2000), various literature reported the migration velocity, v [m/s], to scale with saturated transport on a flat bed, and the inverse of the dune size (Durán et al., 2010):

$$v \approx \alpha q_{sat,0}/W \tag{10}$$

where $q_{sat,0}$ [m^3/m] is the saturated sediment flux over a flat bed (= $C_{sat,0} \cdot u_{sed,0}$), and constant α being approximately equal to 50 [−].

4.2. Parabolic dunes

Dynamic parabolic dunes are in a transitional state, starting with active barchan dunes with no vegetation towards static vegetated parabolic dunes (Durán et al., 2008). Durán and Herrmann (2006) introduced a fixation index as a measure of dune activity to quantify the balance between the stabilizing influence of vegetation and active sediment transport:

$$\Theta \equiv \frac{q_{sat,0}}{V^{1/3}V_{\text{ver}}} \tag{11}$$

where $V^{1/3}$ is a length scale related to the dune volume V. Durán and Herrmann (2006) found that when $\Theta \gtrsim 0.5$ [−], the impact of the active sediment transport is larger than the fixation by vegetation leading to a non-stabilized dune.

To evaluate the model's ability to simulate the vegetation fixation-mobilization balance, three parabolic dunes are simulated, each with differing rates of vegetation growth (V_{ver}) at 3.5, 6.0, and 8.5 m/year. A constant wind speed of 10 m/s in a positive x-direction is used. In this case, both wind conditions and vegetation growth rates solely serve an academic objective. These wind speeds and growth rates correspond to fixation indices θ of approximately 0.85, 0.50, and 0.35, respectively.

For a quantitative model validation, the 'real-world' conditions along the coast of Ceará in Brazil are simulated (see Fig. 2b). This coastline is characterized by many sections covered with coastal dunes experiencing varying levels of stabilization (Durán et al., 2008). The wind conditions for the simulation are derived for the 1995–1999 period, preceding the measurements by Sauermann et al. (2000). The period from July to December is characterized by dry, windy conditions favourable for dune mobilization, while January to June marks the rainy season, typically featuring winds below the threshold velocity for aeolian transport. In two different simulations, vegetation growth is modelled at a constant 0.18 and 0.25 m/year. Therefore, the influence of seasonal abiotic factors like rainfall and temperature on vegetation growth is ignored. The initial topography replicates a cone-shaped feature, with the initial volume set to match the volumes by Sauermann et al. (2000). The landform's centre of gravity is tracked to determine the migration velocity over a simulation period of 40 years. To our knowledge, no measurement data is available over such extensive periods. Therefore, validation is primarily based on typical migration rates mentioned in literature (Goudie, 2011).

4.3. Embryo dunes

In coastal environments, marine influences on aeolian sediment transport and vegetation significantly impact the ecomorphological development of landforms. The presence of a waterline is lacking in both barchan and parabolic dune simulations. To assess the model's ability to describe dune development in a coastal setting, the formation of an embryo dune field under marine influences is simulated. Our simulation is based on observations of an embryo dune field along the coast of the island Texel, Netherlands (van Puijenbroek et al., 2017c). Drone photography was used to construct digital elevation models, encompassing a summer and a winter season.

We attempt to reproduce the observations by van Puijenbroek et al. (2017c) by simulating a flat, sloping beach with randomized vegetation establishment and the presence of a waterline. The simulation period is 5 years. Water levels and wave conditions are obtained from Rijkswaterstaat's Waterinfo database at Eurogeul (Rijkswaterstaat, 2024), located ≈ 100 km south of the location of interest. A non-erodible layer is implemented just below the initial bed level ($z_{ne} = z_{B,0} - 0.1$), stabilizing the coastal profile. The bed levels in submerged cells are gradually reset to their original elevation, compensating for aeolian erosion and replicating marine-driven supply into the intertidal zone. The model's implementation of storm erosion lacks an accurate description of sediment transport due to surf- and swash-related processes. Therefore, it is unrealistic to expect accurate reproduction of the removal of embryo dune features.

The model assumes a vegetation establishment probability of 0.05 [year^{-1}m^{-2}] and lateral vegetation spread at 0.2 [year^{-1}m^{-2}], aligning with the model settings of DUBEVEG in Keijsers et al. (2016). Once cells are submerged, vegetation is removed. To restrict our focus to the establishment and removal of vegetation, the vertical vegetation growth V_{ver} is set at 10 m/year, meaning that vegetation can outgrow any burial rate. A benchmark simulation, without vegetation establishment, is conducted to validate the onshore aeolian transport flux, yielding an average influx of ≈16 m^3/m/year, lower than the findings by van Puijenbroek et al. (2017c) at ≈ 30 m^3/m/year.

The validation is aimed at qualitatively reproducing the seasonal variability in dune establishment, removal and growth. Additionally, we want to assess whether the model is capable of reproducing the sheltering effect of other dunes on growth as found by van Puijenbroek et al. (2017c).

4.4. Blowouts

The blowout simulation is based on the evolution of five foredune notches located in National Park Zuid-Kennemerland (NPZK), the Netherlands (see Fig. 2d). We attempt to simulate the geomorphic response of this coastal area after the excavation of the notches as examined by Ruessink et al. (2018). The simulation is set up for 10 years (2013–2023), extending upon the evaluation period by Ruessink et al. (2018). The initial topography obtained from DEMs is built upon LiDAR measurements of the Dutch dunes (Bochev-Van der Burgh et al., 2011). The water level variations and wave conditions are obtained from an observation station at Eurogeul (Rijkswaterstaat, 2024).

For the sake of applicability and reproducibility, the model complexity is reduced by making some heuristic assumptions. The groundwater table is located 0.1 meters below the initial bed level across the domain, similar to the embryo dune simulations. This prevents erosion from the upper beachface, while sediment availability is ensured in the intertidal area by resetting the bed level elevation of submerged cells. Additionally, the groundwater has a maximum level of 5.5 m+NAP, setting a maximum erosion depth within the blowout features. The vegetation density ρ_{veg} is set to 1.0 [−] landward of the dunefoot (2 m+NAP), while the notches are non-vegetated. The vertical growth rate of vegetation V_{ver} is set to be 3 m/year. This growth rate is slightly higher compared to marram grass typically found along the Dutch coast, to ensure the foredune vegetation survives high deposition rates. The ability of the vegetation to re-establish is excluded by turning off lateral growth and germination, disabling blowout closure. To replicate the stabilizing effect of roots on the sediment, the angle of repose is increased to 44° The separation bubble is disabled, as the implementation is deemed not suitable for such a complex and dynamic coastal environment. The computational domain, vegetation coverage and initial topography are shown in Fig. 5.

For validation, the simulated bed level change is compared with the measured annual topography (Bochev-Van der Burgh et al., 2011). All data points that could potentially be inundated (<2 m+NAP) are filtered out of the measurement data to prevent inconsistencies due
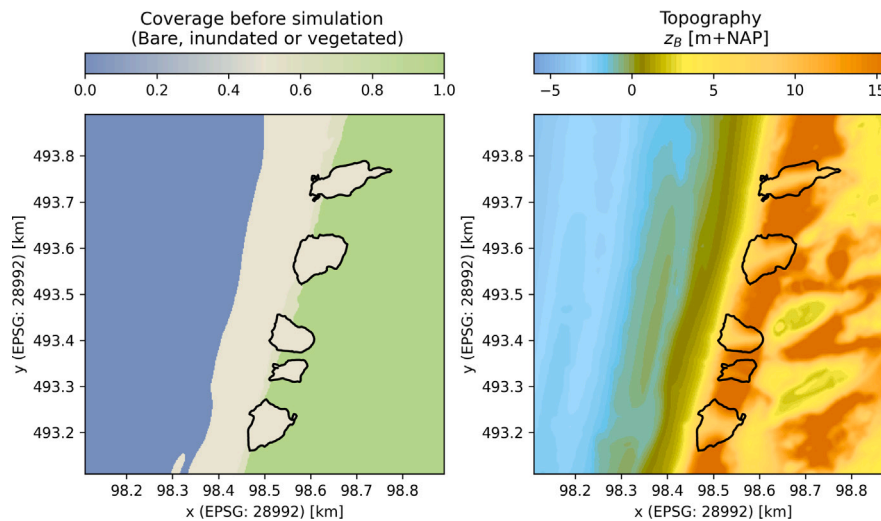
Fig. 5. Setup of a simulation of five excavated notches at the National Park Zuid-Kennemerland (NPZK). The left panel shows the sand coverage, being inundated (blue), vegetated (green) or bare (yellow) at the beginning of the simulation. The right panel shows the initial bed levels based on LiDAR measurements.

to ocean surface reflections. The simulation and measurement results are visually compared and analysis of the erosional and depositional sediment volumes from the blowouts into the backdune is carried out for a quantitative validation.

5. Results

5.1. Barchan dunes

The results of the barchan dune simulations using academic wind conditions coming from varying directions are presented in Fig. 6. The left panels reveal that the dunes' migration direction and orientation consistently align with the wind direction. The imposed wind direction does not significantly alter the crescentic shape of the dunes. The simulated features are mass conserving. Also, when increasing the directional spread ($\sigma = 0°$ in the left panels to $\sigma = 45°$ in the right panels) a different (less pronounced) crescentic shape was simulated.

The shape and migration velocity of the eight simulated Moroccan barchan dunes, compared with real-world measurements by Sauermann et al. (2000), are depicted in Fig. 7. After 5–10 years of simulation the equilibrium shape of these dunes is achieved (top-left panel of Fig. 7). Dune dimensions are calculated using a rotated coordinate system with the dune's crest as the origin, as shown in the bottom-left panel of Fig. 7. Dune heights vary between 3–9 meters and align with the height-to-volume ratio (h and V) observed by Sauermann et al. (2000). However, the dune length (L) relative to height is slightly underpredicted, as shown in the top-right panel of Fig. 7. The height-to-width (h and W) ratio matches closely with observations by Sauermann et al. (2000), Finkel (1959) and Hastenrath (1967) as shown in the bottom-right panel of Fig. 7.

The migration velocity of the simulated barchan dunes is determined by tracking the location of the dune crest, with the results displayed in the bottom-centre panel of Fig. 7. The findings reveal that the dunes' migration velocity decreases as their size increases, aligning well with the relationship proposed by Durán et al. (2010, Eq. 10).

5.2. Parabolic dunes

The results of the parabolic dune simulations with varying fixation indices are displayed in Fig. 8. The left panels show the simulated sand cover – bare (yellow) or vegetated (green) – based on the vegetation

density ρ_{veg} at corresponding times. The right panels illustrate the topographic result after 4 years. The upper panels illustrate a dune with a vegetation growth V_{ver} of 3.5 m/year, resulting in a fixation index Θ of 0.85 (-), where the dune is mostly unvegetated and migrates windward. This aligns with the observations by Durán and Herrmann (2006) that landforms with a Θ larger than approximately 0.5 are too dynamic to stabilize. Increasing V_{ver} to 6.0 m/year, $\Theta = 0.50$ (-), leads to a more significant fixation of the dune, as shown by the thicker trailing arms and greater vegetated areas in the centre panels. The highest vegetation growth rate simulation ($V_{ver} = 8.5$ m/year), corresponding to the lowest fixation index $\Theta = 0.35$, results in almost immediate dune stabilization. Although this trend of decreasing dynamics with higher vegetation growth aligns with earlier work, the extent of stabilization in these simulations is more severe than reported by Durán and Herrmann (2006) for comparable fixation indices.

The results of the simulated parabolic dune development under real-world Brazilian wind conditions are illustrated in Fig. 9. Generally, parabolic dunes worldwide migrate at velocities ranging from 2 to 7 m/year, as detailed in Goudie (2011). In these simulations, despite neglecting vegetation's dependency on abiotic conditions, the incorporation of real-world wind data introduces seasonal variability. With a vertical vegetation growth, V_{ver}, of 0.18 m/year, the average annual migration rate is between 2–3 m/year, as shown by the blue dotted line in Fig. 9. For a slightly higher V_{ver} of 0.25 m/year, the migration rate decreases over time, leading to near-complete fixation after 40 years, indicated by the orange dotted line in Fig. 9. Also, the simulations include some significant seasonal variability in migration speed. Monthly averages of migration rates reach up to 9 m/year during windy periods. Complete stabilization is simulated in calmer months. This suggests substantial differences in fixation index across seasons.

5.3. Embryo dunes

The simulated initialization, growth, and destruction of embryo dunes are showcased in Fig. 10. The top-left panels illustrate the early establishment of vegetation. Subsequently, vegetation patches begin to grow both vertically and laterally due to sediment deposition and lateral vegetation spread. This leads to an increase in the footprint and volume of the embryo dunes, which gradually coalesce into larger dune formations. The progression of this growth and merging of dunes over time is depicted in the centre and right panels of Fig. 10, corresponding to 2.5 and 4.5 years into the simulation, respectively.
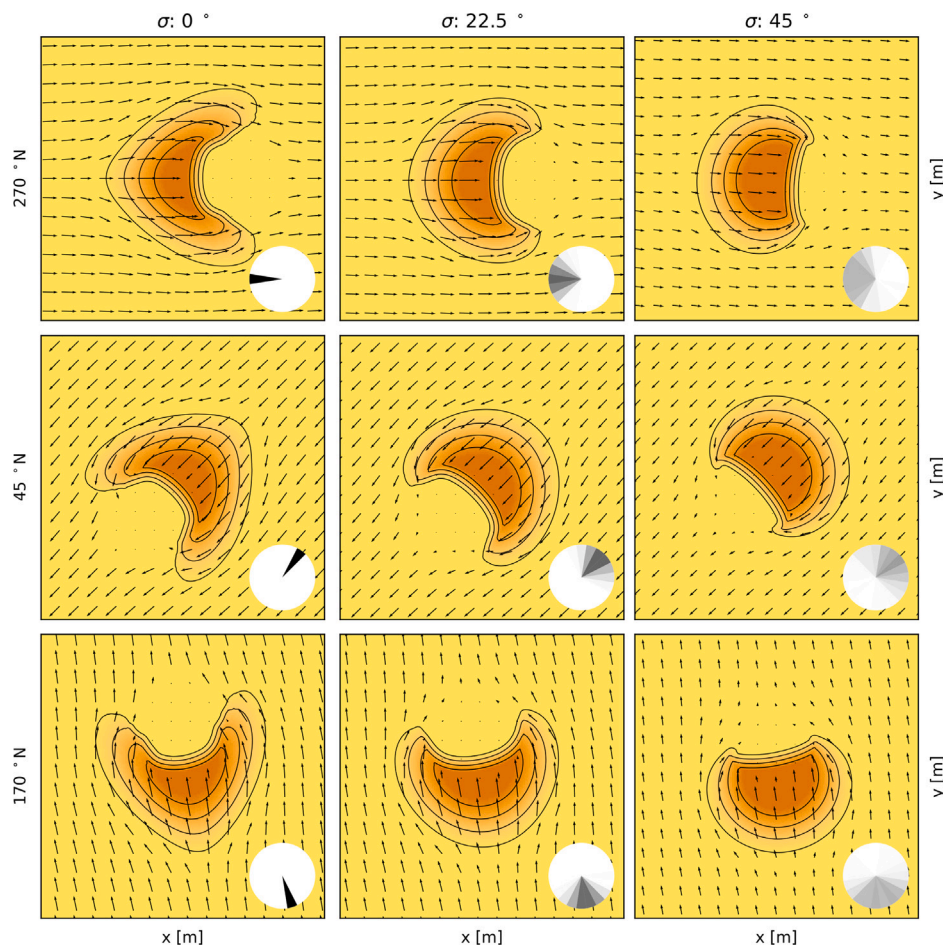
Fig. 6. Demonstration of the model's ability to simulate landforms for wind coming from different directions (top to bottom) and for different spreading rates (left to right).

The third panel of Fig. 10 illustrates the evolution in the number of embryo dunes, highlighting marked developmental differences between dunes in the zone exposed to marine influences and the zone sheltered from marine influences. Exposed dunes see their numbers sharply decrease at the onset of several stormy seasons, particularly during the winter of 2014/2015. Conversely, the count of sheltered dunes steadily rises and stabilizes around 120 after three years. Initially, when the exposed embryo dunes are relatively small, both sheltered and exposed dunes exhibit similar growth rates, as illustrated by their respective weekly volumetric growth ΔV_{dune} shown in the fourth panel. This may suggests that sediment capture by seaward dunes did not significantly affect the sheltered dunes. However, this dynamic changes after the exposed dunes undergo significantly more growth than the sheltered ones in the winter of 2015/2016, likely because they capture the majority of the sediment, limiting the remaining flux towards the sheltered zone. This simulated behaviour is consistent with the findings by van Puijenbroek et al. (2017c), whose measurements occurred in a dune field estimated to be in a similar stage of development – about five years after its initial formation – as the final year of our simulation.

5.4. Blowouts

For the model-data comparison of the developing notches located in National Park Zuid-Kennemerland, the volumetric analysis carried out by Ruessink et al. (2018) is partly reproduced and extended, as displayed in Fig. 11e. Volumetric analysis is carried out based on

three geomorphic units: (1) notches; (2) foredune; (3) backdune; after (Ruessink et al., 2018). The domain is and these respective units are shown in Fig. 11c.

The initiation and early development of the notches in the coastal foredunes along the NPZK region are simulated over a 10-year period. The erosion from the notches, driven by airflow acceleration throughout the blowouts (see arrows in Fig. 11d), is visually similar to observations (Fig. 11a & b). The centre of the blowout erodes up to the assumed non-erodible layer due to soil moisture and most wind-erosion happens at the erosional walls. The simulated volume eroded from the notches corresponds well with the observations (purple line in Fig. 11e). Measurements show much of the eroded sediment to be deposited in the backdune, resulting in an onshore migration of the overall dune volume, as shown by the red patches in Fig. 11a. Although this behaviour is reproduced by the model, the backdune deposition is underpredicted by the model with 62.5% when compared to measurements. As the erosional volume from the notches is slightly overestimated at 25.5%, sediment which is expected to be deposited in the backdune, a limited amount of pick-up from the beachface likely explains the majority of this underprediction in deposition.

6. Discussion

So far, this paper has given a detailed display of the assumptions in the AeoLiS model and the corresponding results for the four particular cases. Barchan dunes, parabolic dunes, embryo dunes and blowouts are simulated using open-source AeoLiS code and, consistent with other
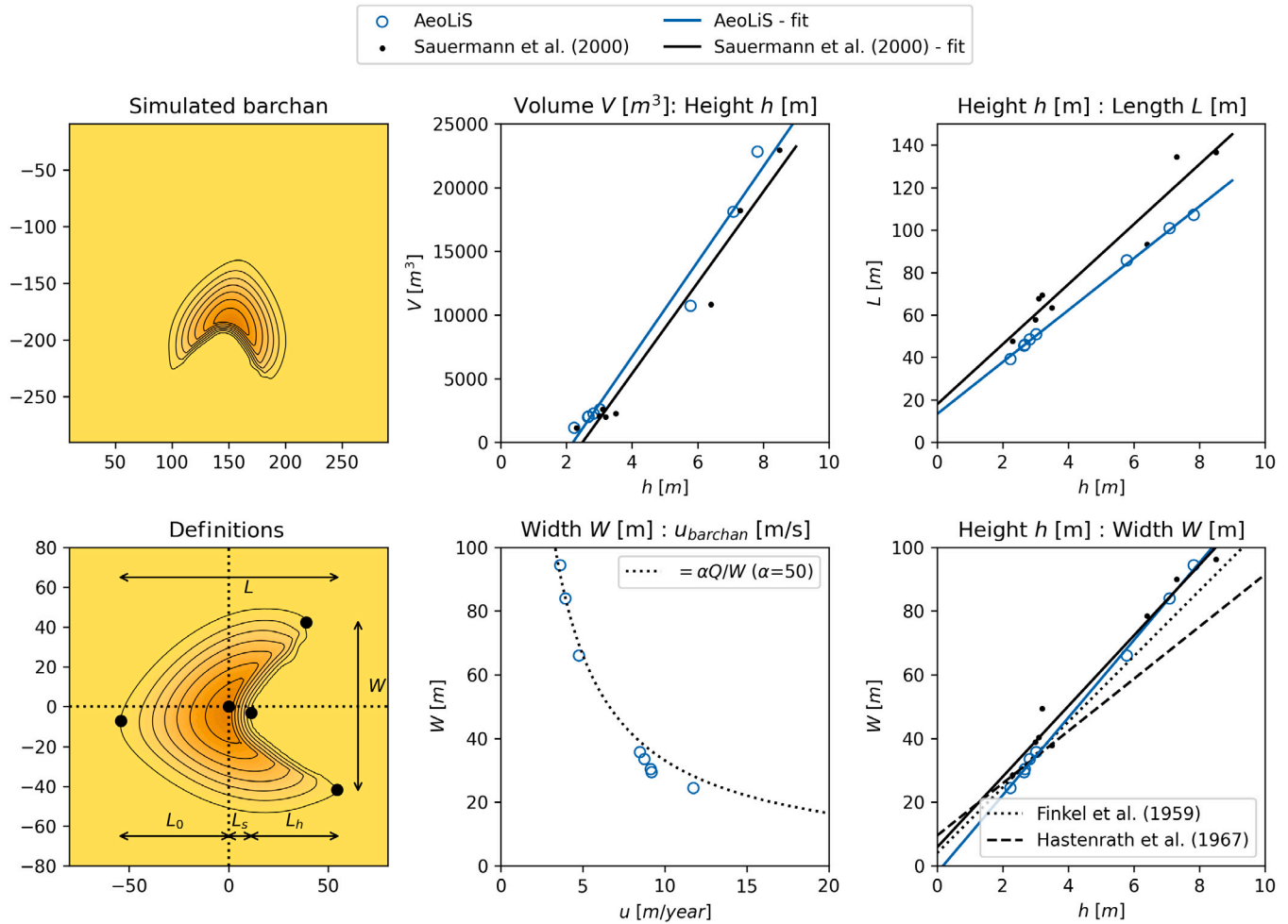
Fig. 7. Quantitative comparison between the simulated and observed volume V, height h, length L and width W for eight barchan dunes located in Morocco, as measured by Sauermann et al. (2000), Finkel (1959), Hastenrath (1967). The migration velocity is compared with a relation proposed by Durán et al. (2010, Eq. (2.10)).

applications in the literature, implementing the relevant physics for each case (e.g., vegetation dynamics, multidirectional winds, shear, non-erodible layers) to generate morphological forms as observed in nature. The model reproduced the crescentic shape of barchan dunes, with the spatial dimensions' ratios matching those recorded in earlier studies (Finkel, 1959; Hastenrath, 1967; Hesp and Hastings, 1998; Sauermann et al., 2000; Hersen, 2004). This outcome gives confidence in the model's new topographic steering process, as adopted from Durán and Moore (2013) with the exception that a custom grid rotation scheme implemented in AeoLiS allows for multidirectional winds. This capability is particularly necessary for accurate simulation of real world dune modelling applications, where wind directions are highly variable and for which wind direction has critical implications both of sediment input into dune complexes (e.g., Delgado-Fernandez, 2010) and on wind flow patterns over the dune form (e.g., Kombiadou et al., 2023; Hesp and Smyth, 2021).

Whereas the original AeoLiS model presented by Hoonhout and de Vries (2016) included multifraction sediment transport processes and various supply limiters, the model at the time did not include capabilities to simulate the full suite of processes that result in aeolian sediment transport gradients that contribute to net landform change. In coastal environments, vegetation is one of the most effective agents for dune formation. In this study, the transition of dynamic crescentic dunes into u-shaped parabolic dunes was successfully simulated

through a simple representation of vegetation growth and the interaction with shear stress (Anthonsen et al., 1996; Durán et al., 2008; Reitz et al., 2010; Barchyn and Hugenholtz, 2012).

In the blowout simulation illustrated in Fig. 11, the model effectively replicated observed erosion and deposition patterns in both spatial and volumetric terms (Ruessink et al., 2018). Historically, artificial blowout projects have had mixed success, often due to limited impacts on dune systems or natural infilling post-excavation (Arens et al., 2013; Castelle et al., 2019; Riksen et al., 2016). The prediction of dune responses to such interventions could inform decision-making in terms of excavation volume, location, timing, and combining with other measures.

The presented model may open new possibilities in the field of coastal engineering, landscape management and -planning. However some limitations in its current implementations remain. Especially when accurately reproducing real-world landforms in specific situations. The blowout simulation, despite illustrating the model's collective advancements, also exhibits most of the assumptions that involve limitations. Future updates of the model may include enhanced descriptions of relevant processes, with several key areas identified for further improvement:

- *Complex wind fields* — The model cannot describe complex wind fields that go beyond the scope of Weng et al. (1991)'s theory.
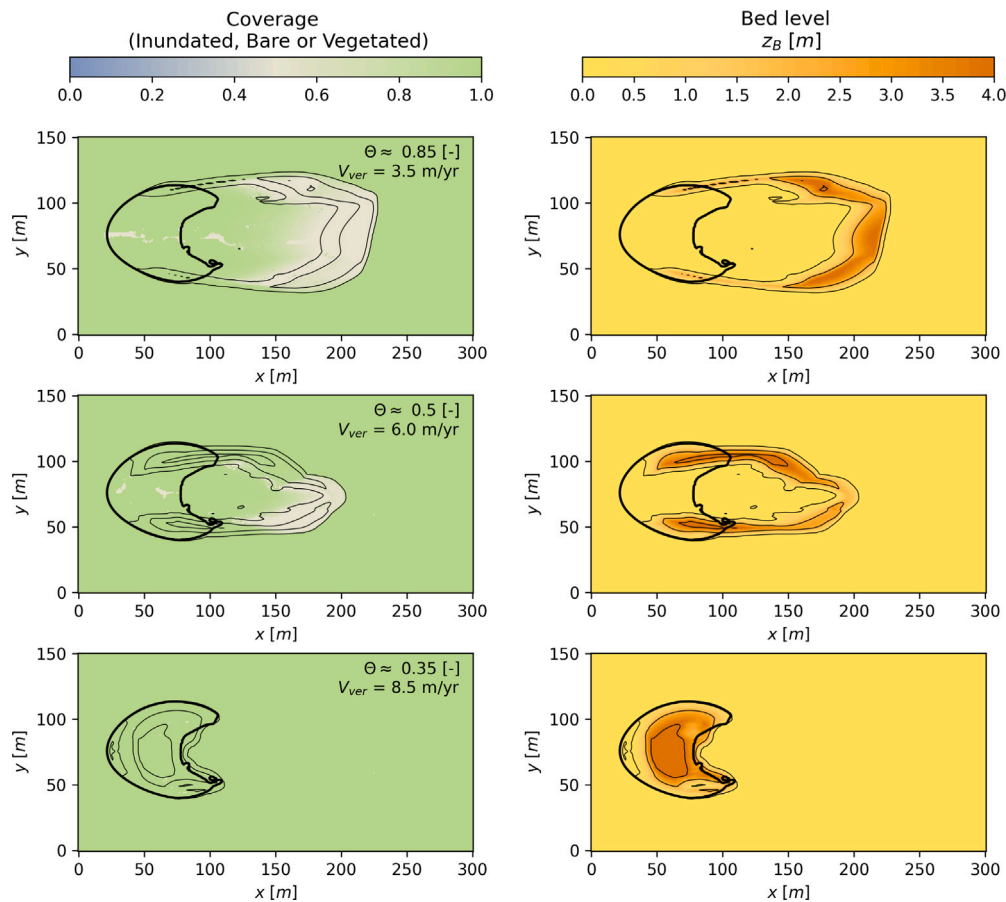
Fig. 8. Simulation overview of three simulated parabolic dunes for varying settings of fixation index ($\Theta \approx 0.85$, 0.50, and 0.35 [−]) by varying vegetation growth speed (V_{ver}: 3.5, 6.0, and 8.5 m/year, resp.). See Video 2 for animated simulation results.

Flow structures around steep topographic gradients and flow reversal on the lee side of dunes are observed in field studies (Lynch et al., 2009) but cannot be described by the current code. Additionally, while the existing analytical shear stress theory allows for rapid computation, low slope assumptions of this formulation may require more complex numerical approaches to effectively simulate wind flow dynamics over steep or complex terrain (e.g., Cecil et al., 2024). However, vegetation roughness is likely to be dominant over the effect of topographic steering. Therefore, the implications of this particular limitation are expected to be limited for typical vegetated foredunes.

- *Avalanching* — The model's constant angle of repose is an important assumption for the avalanching process. However, it does not account for potential variations in the angle of repose due to sediment characteristics, moisture, or vegetation root systems. These parameters may influence slope stability and avalanching processes (Rahn, 1969; Davis et al., 2024). This limitation is illustrated by our need to adjust the angle of repose across the entire domain, as a means to at least partially incorporate the impact of vegetation and root systems on stability.

- *Vegetation growth* — The model's representation of vegetation growth and its interaction with morphodynamics is simplified to a limited set of parameters and processes. The response of vegetation to burial (Nolet et al., 2018), as well as the influence of other abiotic factors like salinity, drought, and temperature on vegetation growth (van Puijenbroek et al., 2017a; Homberger et al., 2024) could be elaborated in future modelling efforts. This

knowledge gap in vegetation modelling was highlighted during the blowout simulation which required significant calibration to achieve realistic outcomes. And yet, erosion and deposition patterns still deviated from actual observations (Dickey et al., 2023).

- *Multiple species* — The current model supports only one type of vegetation characteristic, whereas multiple species with distinct growth functions may be needed for alternative landform simulations (Baas and Nield, 2007). This factor may be especially important in coastal settings where mixed species plots are common on natural coastal foredunes and differing plant species have widely differing morphological characteristics (e.g., Goldstein et al., 2018; Walker and Zinnert, 2022).

- *Removal and establishment* — The binary approach for vegetation establishment and removal in the model does not reflect the gradual erosion and persistence of vegetation in natural settings. The model could incorporate the influence of seed dispersal and various abiotic conditions on vegetation establishment. Additionally, it seems improbable that transient inundation would be immediately fatal to vegetation. Enhancing the implementation of vegetation response to hydrodynamic stresses could improve the inclusion of vegetation zoning.

- *Supply-limitations* — The underestimation of onshore aeolian flux in the embryo dune and blowout simulations, though not directly related to landform shaping processes, highlights the critical need for precise modelling of sediment supply on the beach face. Accurately capturing this aspect is essential, as inaccuracies can significantly impact the outcome of landform simulations.
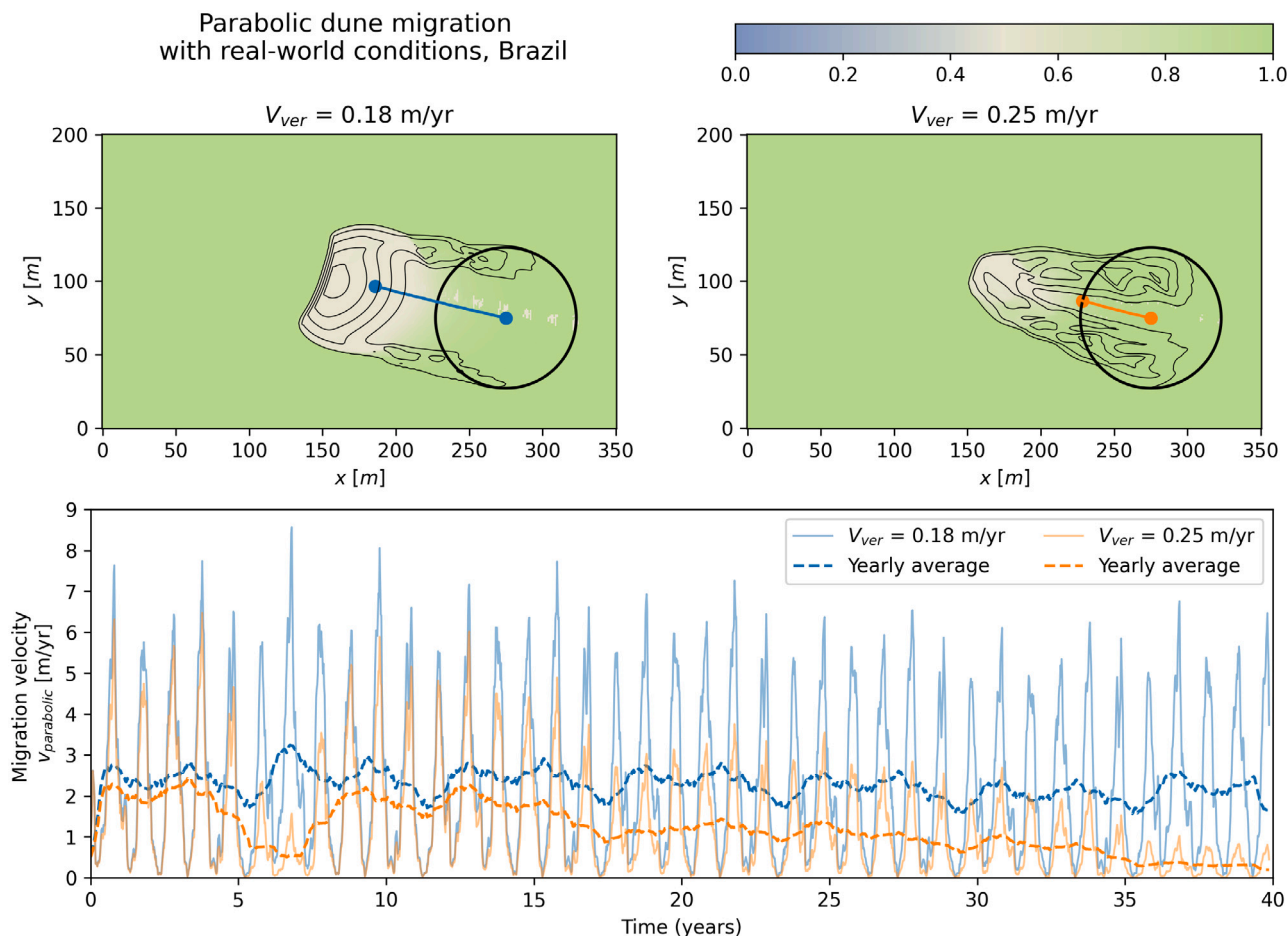
Fig. 9. Migration of parabolic dunes under real-world, Brazilian, wind conditions. The centre of both dunes is traced, as indicated by the blue and orange lines in the upper panels. The lower panel displays the monthly (continuous) and yearly (dotted) averaged migration rates for both simulations.

Despite these limitations, the AeoLiS model has made contributions to several engineering projects. The Sand Engine mega-nourishment in the Netherlands was designed to develop in a dynamic coastal dune landscape over several decades (Stive et al., 2013). Simulations by Hoonhout and de Vries (2019) have explained the spatiotemporal distributions of sediment at the site. These simulations have been used to evaluate its design and make management decisions related to beach nourishment and dune management along the Dutch coast. Leveraging a subset of the model advancements presented in this manuscript, van Westen et al. (2024) further extended the model domain alongshore, increased spatial resolution, and coupled the model with a hydrodynamic model component to introduce the interplay between aeolian- and marine-driven morphological change. This enabled the inclusion of marine-driven impact on beach width, sediment availability and dune growth. A growing set of use applied engineering use cases is now possible given new capabilities included within AeoLiS that allow for aeolian transport and related morphological changes to be simulated across broad spatial scales (meters to kilometers; e.g., Fig. 11), temporal scales (e.g., days to decades), and including a range of physical and ecological processes. Continued demonstration and assessment of capabilities for simulating real-world 1D and 2D profile change will further enable the use of AeoLiS as a practical tool for engineering planning and design work related to managing sediment transport pathways and/or optimizing landform evolution in coastal systems to add flood or ecosystem service benefits.

7. Conclusion

The AeoLiS model provides an implementation of a quantitative set of process-based descriptions regarding wind-flow, aeolian sediment transport, vegetation growth, submersion and the feedback with coastal morphology. The model is built on the principle of supply-limited aeolian sediment transport where wind shear and surface characteristics determine sediment transports that cause morphological changes. The model is forced with wind speed, water levels and wave heights as boundary conditions and solves for intrinsic process interactions related to morphology, vegetation growth and topographic steering of wind flow. Assumptions can be varied depending on the specific goal of the simulation.

Several characteristic aeolian (coastal) landform shapes can be simulated using the novel implementations in the AeoLiS model. Barchan dunes can be simulated by combining assumptions that describe aeolian sediment transport, topographic steering and avalanching. Comparison with real-world measurements of barchan dunes located in Morocco gives confidence in the model to simulate landform development under realistic wind conditions.

Parabolic dunes can be simulated when taking into account the description of vegetation development and extending the temporal scale of the barchan dune simulation. The establishment of vegetation on the relatively stable sides of the dune causes further stabilization and the subsequent development into a parabolic-shaped dune corresponds well with the literature, as do simulated migration rates.
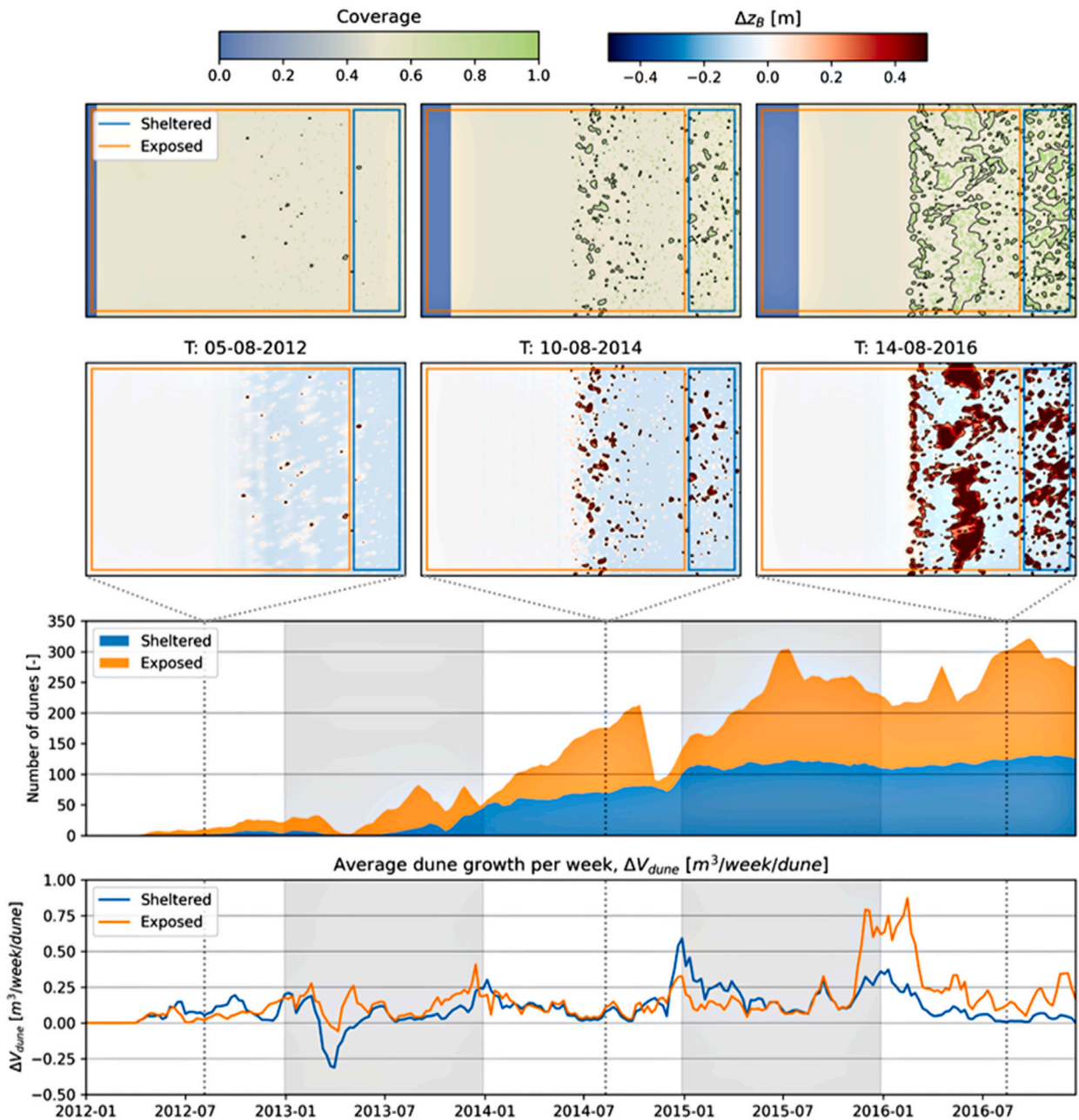
Fig. 10. Simulation overview of the development of an embryonic dune field, including vegetation establishment, growth, propagation, and destruction.

Embryo dunes are simulated by adding a probabilistic approach to vegetation establishment and lateral propagation and the influence of swash processes in the domain. The simulated behaviour in seasonal variation and the sheltering impact of seaward-located dunes are similar to earlier measurements carried out at the Hors, Texel, The Netherlands.

The model's applicability in practical engineering cases is demonstrated by simulating the development of five foredune notches along the Dutch coast. The simulated spatial pattern and volumetric landward movement of sediment show that the combined implementation of the presented processes is capable of describing real-world coastal dune development on engineering spatiotemporal scales.

Although the AeoLiS model can describe several theoretical and practical behaviours of coastal aeolian dune landscapes, the implementation of some additional assumptions may improve the model's predictive capability. Examples are (amongst others) the implementation of different vegetation species or secondary flow patterns.

The AeoLiS model is openly accessible and all results in this publication are reproducible in the open source domain. This way we aim to underscore AeoLiS' potential as a basis for collaborative development towards a more comprehensive description of coastal dunes.
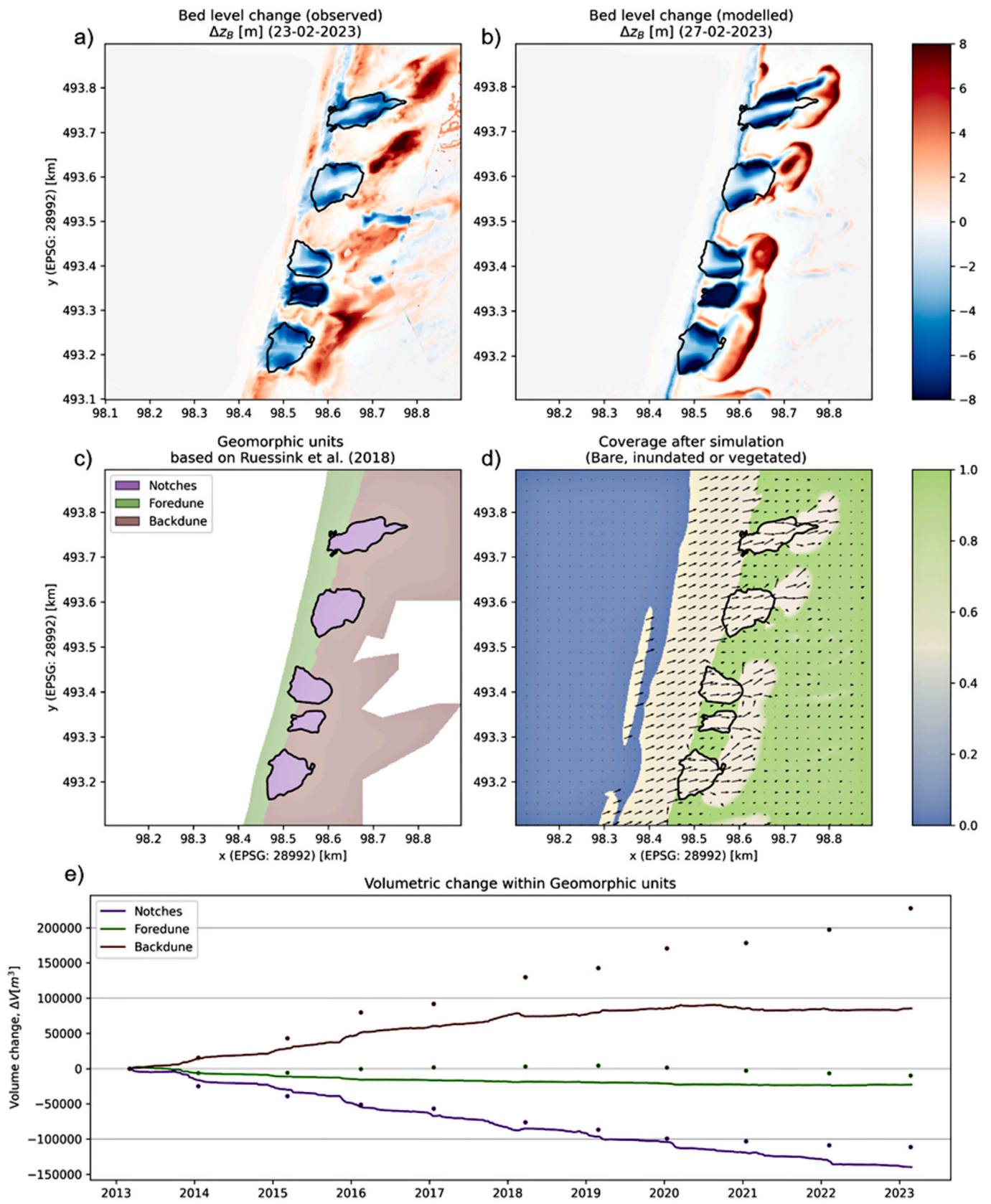
Fig. 11. Comparison between model outcomes and measurements. The observed (a) and modelled (b) erosion (blue) and sedimentation (red) patterns are compared. Panel (c) shows the three defined units for which the volumetric change is computed. The outcomes of the volumetric comparison are shown over time in panel (e). See Video 3 for animated simulation results.

CRediT authorship contribution statement

Bart van Westen: Writing – review & editing, Writing – original draft, Visualization, Software, Methodology, Conceptualization. **Sierd de Vries:** Writing – review & editing, Writing – original draft, Supervision, Software, Methodology, Funding acquisition, Conceptualization. **Nicholas Cohn:** Writing – review & editing, Software, Conceptualization. **Christa van IJzendoorn:** Writing – review & editing, Software. **Glenn Strypsteen:** Writing – review & editing, Software. **Caroline Hallin:** Writing – review & editing, Software.

Declaration of competing interest

The authors declare that they have no known competing financial interests or personal relationships that could have appeared to influence the work reported in this paper.

Data availability

The link to the AeoLiS code and model configuration is included in the manuscript under Software Availability.

Acknowledgements

Software availability

AeoLiS by de Vries et al. (2023) was used in this work for sediment transport calculations. Software is openly available from https://github.com/openearth/aeolis-python/tree/deVries2023. All examples (see Table B.1) can be reproduced using the input files in the examples folder on the AeoLiS Github (https://github.com/openearth/aeolis-python/tree/deVries2023/aeolis/examples/vanWesten2024). In addition, the configuration files provide an overview of the values of the relevant model parameters. A more elaborate description and the default values of all parameters is listed on AeoLiS' Read the Docs (https://aeolis.readthedocs.io/en/latest/user/defaults.html).

Appendix A. Topographic steering

The shear stress perturbation in the x- and y-directions ($\delta \tau_x$ and $\delta \tau_y$) is computed in Fourier space according to the following equations:

$$\delta \tilde{\tau}_x(\vec{k}) = \frac{2 \tilde{z}_b(\vec{k})}{U^2(l)} \frac{k_x^2}{|\vec{k}|} \left\{ -1 + \left(2 \ln \frac{l}{z_0'} + \frac{|k|^2}{k_x^2} \right) \sigma \frac{K_1(2\sigma)}{K_0(2\sigma)} \right\} \quad \text{(A.1)}$$

$$\delta \tilde{\tau}_y(\vec{k}) = \frac{2 \tilde{z}_b(\vec{k})}{U^2(l)} \frac{k_x k_y}{|\vec{k}|} 2 \sqrt{2} \sigma K_1(2\sqrt{2}\sigma) \quad \text{(A.2)}$$

$$\sigma = \sqrt{i L k_x z_0'/l} \quad \text{(A.3)}$$

where ˜ indicates the Fourier-transformed components of the parameters, k_x and k_y are the components of the wave vector $\vec{k}$ in Fourier space
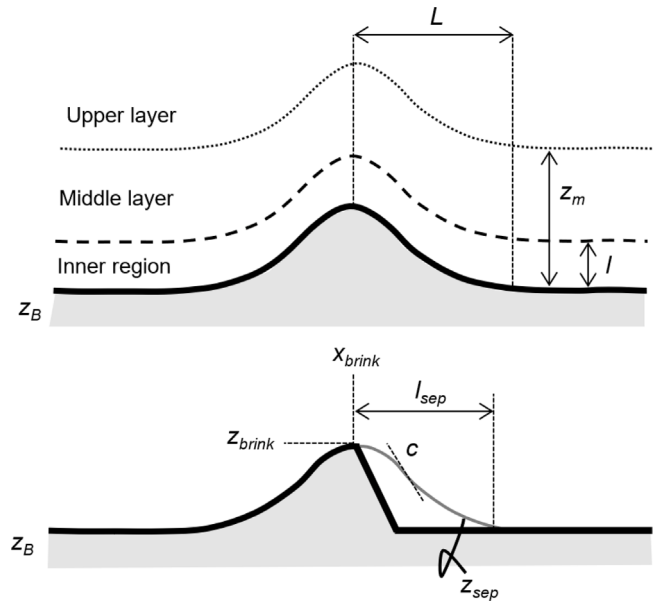

Fig. A.12. Schematic overview of shear perturbation and flow separation approach. Based on Weng et al. (1991) and Kroy et al. (2002).

and K_0 and K_1 are modified Bessel functions. l [m] (see Fig. A.12) is the depth of the inner layer of flow:

$$l = \frac{2\kappa^2 L}{\ln \frac{l}{z_0'}} \quad \text{(A.4)}$$

where L [m] is the typical length scale of the hill. The constant $U(l)$ [−] is the dimensionless vertical velocity profile at height l:

$$U(l) \equiv \frac{\ln \frac{l}{z_0'}}{\ln \frac{z_m}{z_0'}} \quad \text{(A.5)}$$

where z_m [m] is the height of the middle layer of flow:

$$z_m = \sqrt{\frac{L^2}{\ln \frac{z_m}{z_0'}}} \quad \text{(A.6)}$$

For one-dimensional situations, a simplified solution of the shear perturbation approach is implemented, ignoring some minor terms, leading to a less computationally expensive approach (Kroy et al., 2002):

$$\delta \tau = \alpha \int_{-\infty}^{\infty} d\xi \frac{\frac{\delta z_b}{\delta x}(x - \xi)}{\pi \xi} + \beta \frac{\delta z_b}{\delta x}(x) \quad \text{(A.7)}$$

where α [−] and β [−] both depend on L/z_0, but are not computed in the model but are user-defined fixed variables. ξ [−] is the normalized cross-shore distance x/L.

The separation bubble surface z_{sep} [m] is modelled by a third-order polynomial. The dimensions of the separation bubble are shown in A.12. The height of the brinkline, or the location where the separation bubble starts to detach from the bed, is defined by $z_b(x_{\text{brink}}) \equiv z_{\text{brink}}$.

Assuming a maximum slope c [deg] for the separation surface, determining the shape of the separation bubble, the reattachment length l is obtained by:

$$l \approx \frac{3 z_{\text{brink}}}{2c} \left(1 + \frac{z_{\text{brink}}}{4c} + 2 \left(\frac{z_{\text{brink}}}{4c} \right)^2 \right) \quad \text{(A.8)}$$

The separation bubble z_{sep} is calculated as:

$$z_{sep}(x) = a_3(x - x_{brink})^3 + a_2(x - x_{brink})^2 + z'_{brink}(x - x_{brink}) + z_{brink} \quad \text{(A.9)}$$

Table B.1
Overview of all landform simulations performed within this study.

Landform	Sim. name	Figure
Demonstrating the model's ability to describe ...		
Barchan dunes (Section 5.1)		Video 4
... barchan dune development under varying wind direction and spreading.	1. barchan_[a1..c3]	Fig. 6
... realistic barchan shapes and migration under Moroccan wind conditions.	2. barchan_[m1..m8]	Fig. 7
Parabolic (Section 5.2)		Video 5
... representative stabilization patterns for varying levels of fixation.	3. parabolic_[a1..a3]	Fig. 8
... a realistic migration velocity under Brazilian wind conditions.	4. parabolic_[b1,b2]	Fig. 9
Embryo dunes (Section 5.3)		Video 6
... vegetation establishment and the initial phase of dune formation.	5. embryo	Fig. 10
Blowouts (Section 5.4)		Video 7
... the development of real-world foredune notches along the Dutch coast.	6. blowouts	Fig. 11

where:

$$a_2 = -\frac{3z_{brink} + 2z'_{brink}l}{l^2} \tag{A.10}$$

$$a_3 = \frac{2z_{brink} + z'_{brink}l}{l^3} \tag{A.11}$$

Appendix B. Simulation overview

See Table B.1.

Appendix C. Supplementary data

The animation videos referred to in the text can be accessed in the supplementary material online at https://doi.org/10.1016/j.envsoft.2024.106093.

References

Anthonsen, K.L., Clemmensen, L.B., Jensen, J.H., 1996. Evolution of a dune from crescentic to parabolic form in response to short-term climatic changes: Råbjerg mile, skagen odde, Denmark. Geomorphology 17 (1), 63–77, Response of Aeolian Processes to Global Change.

Arens, S., 1996. Patterns of sand transport on vegetated foredunes. Geomorphology 17 (4), 339–350.

Arens, S.M., Mulder, J.P., Slings, Q.L., Geelen, L.H., Damsma, P., 2013. Dynamic dune management, integrating objectives of nature development and coastal safety: Examples from the netherlands. Geomorphology 199, 205–213.

Arens, S.M., de Vries, S., Geelen, L.H., Ruessink, G., van der Hagen, H.G., Groenendijk, D., 2020. Comment on 'is 're-mobilisation'nature restoration or nature destruction? A commentary'by I. Delgado-fernandez, RGD davidson-arnott & PA hesp. J. Coast. Conserv. 24, 1–4.

Baas, A.C.W., Nield, J.M., 2007. Modelling vegetated dune landscapes. Geophys. Res. Lett. 34 (6).

Bagnold, R.A., 1937. The transport of sand by wind. Geogr. J. 89 (5), 409–438.

Bakker, M.A., van Heteren, S., Vonhögen, L.M., van der Spek, A.J., Van der Valk, B., 2012. Recent coastal dune development: effects of sand nourishments. J. Coast. Res. 28 (3), 587–601.

Bakker, T.W., Stuyfzand, P.J., 1993. Nature conservation and extraction of drinking water in coastal dunes: the meijendel area. In: Landscape Ecology of a Stressed Environment. Springer, pp. 244–262.

Barbier, E.B., Hacker, S.D., Kennedy, C., Koch, E.W., Stier, A.C., Silliman, B.R., 2011. The value of estuarine and coastal ecosystem services. Ecol. Monographs 81 (2), 169–193.

Barchyn, T.E., Hugenholtz, C.H., 2012. A process-based hypothesis for the barchan–parabolic transformation and implications for dune activity modelling. Earth Surf. Process. Landf. 37 (13), 1456–1462.

Bauer, B.O., 1991. Aeolian decoupling of beach sediments. Ann. Assoc. Am. Geogr. 81 (2), 290–303.

Bauer, B., Davidson-Arnott, R., Hesp, P., Namikas, S., Ollerhead, J., Walker, I., 2009. Aeolian sediment transport on a beach: Surface moisture, wind fetch, and mean transport. Geomorphology 105 (1–2), 106–116.

Bauer, B.O., Davidson-Arnott, R.G., Walker, I.J., Hesp, P.A., Ollerhead, J., 2012. Wind direction and complex sediment transport response across a beach–dune system. Earth Surf. Process. Landf. 37 (15), 1661–1677.

Bauer, B.O., Wakes, S.J., 2022. CFD simulations of wind flow across scarped foredunes: Implications for sediment pathways and beach–dune recovery after storms. Earth Surf. Process. Landf. 47 (12), 2989–3015.

Biel, R.G., Hacker, S.D., Ruggiero, P., Cohn, N., Seabloom, E.W., 2017. Coastal protection and conservation on sandy beaches and dunes: context-dependent tradeoffs in ecosystem service supply. Ecosphere 8 (4), e01791.

van der Biest, K., De Nocker, L., Provoost, S., Boerema, A., Staes, J., Meire, P., 2017. Dune dynamics safeguard ecosystem services. Ocean Coast. Manag. 149, 148–158.

Bonte, D., Batsleer, F., Provoost, S., Reijers, V., Vandeghuchte, M.L., Van De Walle, R., Dan, S., Matheve, H., Rauwoens, P., Strypsteen, G., et al., 2021. Biomorphogenic feedbacks and the spatial organization of a dominant grass steer dune development. Front. Ecol. Evol. 670.

Borsje, B.W., van Wesenbeeck, B.K., Dekker, F., Paalvast, P., Bouma, T.J., van Katwijk, M.M., de Vries, M.B., 2011. How ecological engineering can serve in coastal protection. Ecol. Eng. 37 (2), 113–122.

van Boxel, J., Jungerius, P., Kieffer, N., Hampele, N., 1997. Ecological effects of reactivation of artificially stabilized blowouts in coastal dunes. J. Coast. Conserv. 3, 57–62.

Brand, E., Ramaekers, G., Lodder, Q., 2022. Dutch experience with sand nourishments for dynamic coastline conservation–an operational overview. Ocean Coast. Manag. 217, 106008.

Brodie, K., Conery, I., Cohn, N., Spore, N., Palmsten, M., 2019. Spatial variability of coastal foredune evolution, part a: Timescales of months to years. J. Mar. Sci. Eng. 7 (5), 124.

Bochev-Van der Burgh, L., Wijnberg, K.M., Hulscher, S.J., 2011. Decadal-scale morphologic variability of managed coastal dunes. Coast. Eng. 58 (9), 927–936.

Carter, R., 1976. Formation, maintenance and geomorphological significance of an aeolian shell pavement. J. Sediment. Res. 46 (2), 418–429.

Castelle, B., Laporte-Fauret, Q., Marieu, V., Michalet, R., Rosebery, D., Bujan, S., Lubac, B., Bernard, J.-B., Valance, A., Dupont, P., et al., 2019. Nature-based solution along high-energy eroding sandy coasts: preliminary tests on the reinstatement of natural dynamics in reprofiled coastal dunes. Water 11 (12), 2518.

Cecil, O., Cohn, N., Farthing, M., Dutta, S., Trautz, A., 2024. Examination of analytical shear stress predictions for coastal dune evolution. EGUsphere 2024, 1–34.

Cohn, N., Ruggiero, P., de Vries, S., Kaminsky, G.M., 2018. New insights on coastal foredune growth: The relative contributions of marine and aeolian processes. Geophys. Res. Lett. 45 (10), 4965–4973.

Cooper, A., Jackson, D., 2021. Dune gardening? A critical view of the contemporary coastal dune management paradigm. Area 53 (2), 345–352.

Davidson, S.G., Hesp, P.A., DaSilva, M., Da Silva, G.M., 2022. Flow dynamics over a high, steep, erosional coastal dune slope. Geomorphology 402, 108111.

Davidson-Arnott, R.G., Law, M.N., 1996. Measurement and prediction of long-term sediment supply to coastal foredunes. J. Coast. Res. 654–663.

Davis, E.H., Hein, C.J., Cohn, N., White, A.E., Zinnert, J.C., 2024. Differences in internal sedimentologic and biotic structure between natural, managed, and constructed coastal foredunes. Geomorphology 109083.

Delgado-Fernandez, I., 2010. A review of the application of the fetch effect to modelling sand supply to coastal foredunes. Aeolian Res. 2 (2–3), 61–70.

Delgado-Fernandez, I., Davidson-Arnott, R.G., Hesp, P.A., 2019. Is 're-mobilisation'nature restoration or nature destruction? A commentary. J. Coast. Conserv. 23, 1093–1103.

Derijckere, J., Strypsteen, G., Rauwoens, P., 2022. Initial development of an artificial dune: Dune-in-front-of-a-dike site ostend oosteroever-Belgium. p. 18, NCK Days 2022, Date: 2022/03/16-2022/03/18, Location: Enschede, The Netherlands, Netherlands Centre for Coastal Research.

Derijckere, J., Strypsteen, G., Rauwoens, P., 2023. Early-stage development of an artificial dune with varying plant density and distribution. Geomorphology 437, 108806.

Dickey, J., Wengrove, M., Cohn, N., Ruggiero, P., Hacker, S.D., 2023. Observations and modeling of shear stress reduction and sediment flux within sparse dune grass canopies on managed coastal dunes. Earth Surf. Process. Landf. 48 (5), 907–922.

Durán, O., 2007. Vegetated dunes and barchan dune fields (Ph.D. thesis). Universität Stuttgart.

Durán, O., Herrmann, H.J., 2006. Vegetation against dune mobility. Phys. Rev. Lett. 97, 188001.

Durán, O., Moore, L.J., 2013. Vegetation controls on the maximum size of coastal dunes. Proc. Natl. Acad. Sci. 110 (43), 17217–17222.

Durán, O., Parteli, E.J., Herrmann, H.J., 2010. A continuous model for sand dunes: Review, new developments and application to barchan dunes and barchan dune fields. Earth Surf. Process. Landf. 35 (13), 1591–1600.

Durán, O., Silva, M., Bezerra, L., Herrmann, H.J., Maia, L., 2008. Measurements and numerical simulations of the degree of activity and vegetation cover on parabolic dunes in north-eastern Brazil. Geomorphology 102 (3–4), 460–471.

Everard, M., Jones, L., Watts, B., 2010. Have we neglected the societal importance of sand dunes? An ecosystem services perspective. Aquat. Conserv. Mar. Freshw. Ecosyst. 20 (4), 476–487.

Finkel, H.J., 1959. The barchans of southern peru. J. Geol. 67 (6), 614–647.

Geelen, L., Kamps, P., Olsthoorn, T., 2017. From overexploitation to sustainable use, an overview of 160 years of water extraction in the amsterdam dunes, the netherlands. J. Coast. Conserv. 21 (5), 657–668.

Goldstein, E.B., Mullins, E.V., Moore, L.J., Biel, R.G., Brown, J.K., Hacker, S.D., Jay, K.R., Mostow, R.S., Ruggiero, P., Zinnert, J.C., 2018. Literature-based latitudinal distribution and possible range shifts of two US east coast dune grass species (uniola paniculata and ammophila breviligulata). PeerJ 6, e4932.

Goudie, A., 2011. Parabolic dunes: distribution, form, morphology and change. Ann. Arid zone 50 (3&4), 1–7.

Hallin, C., van IJzendoorn, C., Homberger, J.M., de Vries, S., 2023a. Simulating surface soil moisture on sandy beaches. Coast. Eng. 185, 104376.

Hallin, C., van IJzendoorn, C., Skaden, J., de Vries, S., 2023b. Evaluation of threshold-based models to account for surface moisture in meso-scale aeolian sediment transport simulations. In: The Proceedings of the Coastal Sediments Conference. pp. 670–683.

Hamdan, M., Refaat, A., Wahed, M.A., 2016. Morphologic characteristics and migration rate assessment of barchan dunes in the southeastern western desert of Egypt. Geomorphology 257, 57–74.

Hastenrath, S.L., 1967. The barchans of the arequipa region, southern peru. Zeitschrift für Geomorphologie 11 (3), 300–331.

Hersbach, H., Bell, B., Berrisford, P., Hirahara, S., Horányi, A., Muñoz-Sabater, J., Nicolas, J., Peubey, C., Radu, R., Schepers, D., et al., 2020. The ERA5 global reanalysis. Q. J. R. Meteorol. Soc. 146 (730), 1999–2049.

Hersen, P., 2004. On the crescentic shape of barchan dunes. Eur. Phys. J. B 37, 507–514.

Hersen, P., Douady, S., Andreotti, B., 2002. Relevant length scale of barchan dunes. Phys. Rev. Lett. 89 (26), 264301.

Hesp, P., 1989. A review of biological and geomorphological processes involved in the initiation and development of incipient foredunes. Proc. Royal Soc. Edinburgh, Section B: Biological Sciences 96, 181–201.

Hesp, P.A., 2002. Foredunes and blowouts: initiation, geomorphology and dynamics. Geomorphology 48 (1), 245–268, 29th Binghamton Geomorphology Symposium: Coastal Geomorphology.

Hesp, P.A., Hastings, K., 1998. Width, height and slope relationships and aerodynamic maintenance of barchans. Geomorphology 22 (2), 193–204.

Hesp, P.A., Smyth, T.A., 2016. Surfzone-beach-dune interactions: Flow and sediment transport across the intertidal beach and backshore. J. Coast. Res. (75), 8–12.

Hesp, P.A., Smyth, T.A., 2017. Nebkha flow dynamics and shadow dune formation. Geomorphology 282, 27–38.

Hesp, P.A., Smyth, T.A., 2021. CFD flow dynamics over model scarps and slopes. Phys. Geogr. 42 (1), 1–24.

Hesp, P.A., Smyth, T.A., Nielsen, P., Walker, I.J., Bauer, B.O., Davidson-Arnott, R., 2015. Flow deflection over a foredune. Geomorphology 230, 64–74.

Homberger, J.-M., Lynch, A., Riksen, M., Limpens, J., 2024. Growth response of dune-building grasses to precipitation. Ecohydrology e2634.

Hoonhout, B.M., de Vries, S., 2016. A process-based model for aeolian sediment transport and spatiotemporal varying sediment availability. J. Geophys. Res: Earth Surf. 121 (8), 1555–1575.

Hoonhout, B., de Vries, S., 2017. Aeolian sediment supply at a mega nourishment. Coast. Eng. 123, 11–20.

Hoonhout, B., de Vries, S., 2019. Simulating spatiotemporal aeolian sediment supply at a mega nourishment. Coast. Eng. 145, 21–35.

Houser, C., 2009. Synchronization of transport and supply in beach-dune interaction. Progress in Phys. Geogr. 33 (6), 733–746.

van IJzendoorn, C.O., Hallin, C., Reniers, A.J.H.M., de Vries, S., 2023. Modeling multi-Fraction Coastal aeolian sediment transport with horizontal and vertical grain-size variability. J. Geophys. Res: Earth Surf. 128 (7), e2023JF007155.

Jackson, D., Beyers, J., Lynch, K., Cooper, J., Baas, A., Delgado-Fernandez, I., 2011. Investigation of three-dimensional wind flow behaviour over coastal dune morphology under offshore winds using computational fluid dynamics (CFD) and ultrasonic anemometry. Earth Surf. Process. Landf. 36 (8), 1113–1124.

Jackson, N.L., Nordstrom, K.F., 2011. Aeolian sediment transport and landforms in managed coastal systems: a review. Aeolian Res. 3 (2), 181–196.

Keijsers, J., De Groot, A., Riksen, M., 2015. Vegetation and sedimentation on coastal foredunes. Geomorphology 228, 723–734.

Keijsers, J., De Groot, A., Riksen, M., 2016. Modeling the biogeomorphic evolution of coastal dunes in response to climate change. J. Geophys. Res: Earth Surf. 121 (6), 1161–1181.

Kombiadou, K., Costas, S., Roelvink, D., 2023. Exploring controls on coastal dune growth through a simplified model. J. Geophys. Res: Earth Surf. 128 (9), e2023JF007080.

Kroon, A., de Schipper, M., de Vries, S., Aarninkhof, S., 2022. Subaqueous and subaerial beach changes after implementation of a mega nourishment in front of a sea dike. J. Mar. Sci. Eng. 10 (8), 1152.

Kroy, K., Sauermann, G., Herrmann, H.J., 2002. Minimal model for aeolian sand dunes. Phys. Rev. E 66 (3), 031302.

van Kuik, N., de Vries, J., Schwarz, C., Ruessink, G., 2022. Surface-area development of foredune trough blowouts and associated parabolic dunes quantified from time series of satellite imagery. Aeolian Res. 57, 100812.

Laporte-Fauret, Q., Castelle, B., Marieu, V., Nicolae-Lerma, A., Rosebery, D., 2022. Foredune blowout formation and subsequent evolution along a chronically eroding high-energy coast. Geomorphology 414, 108398.

Lynch, K., Jackson, D.W., Cooper, J.A.G., 2009. Foredune accretion under offshore winds. Geomorphology 105 (1), 139–146, Contemporary research in aeolian geomorphology.

Martínez, M.L., Hesp, P.A., Gallego-Fernández, J.B., 2013. Coastal dune restoration: trends and perspectives. Restor. Coast. Dunes 323–339.

Martínez, M.L., Psuty, N.P., 2004. Coastal dunes. Springer.

Matias, A., Ferreira, O., Mendes, I., Dias, J.A., Vila-Concejo, A., 2005. Artificial construction of dunes in the south of Portugal. J. Coast. Res. 21 (3), 472–481.

Maun, M.A., 2009. The biology of coastal sand dunes. Oxford University Press.

van der Meulen, F., de Haes, H.U., 1996. Nature conservation and integrated coastal zone management in Europe: present and future. Landsc. Urban Plan. 34 (3–4), 401–410.

Montreuil, A.L., Bullard, J.E., Chandler, J.H., Millett, J., 2013. Decadal and seasonal development of embryo dunes on an accreting macrotidal beach: North lincolnshire, UK. Earth Surf. Process. Landf. 38 (15), 1851–1868.

Nield, J.M., Baas, A.C., 2008. Investigating parabolic and nebkha dune formation using a cellular automaton modelling approach. Earth Surf. Process. Landf. 33 (5), 724–740.

Nolet, C., Van Puijenbroek, M., Suomalainen, J., Limpens, J., Riksen, M., 2018. UAV-imaging to model growth response of marram grass to sand burial: Implications for coastal dune development. Aeolian Res. 31, 50–61.

Nordstrom, K.F., Lampe, R., Vandemark, L.M., 2000. Reestablishing naturally functioning dunes on developed coasts. Environ. Manag. 25, 37–51.

Paola, C., Voller, V.R., 2005. A generalized exner equation for sediment mass balance. J. Geophys. Res: Earth Surf. 110 (F4).

Parteli, E.J., Durán, O., Bourke, M.C., Tsoar, H., Pöschel, T., Herrmann, H., 2014. Origins of barchan dune asymmetry: Insights from numerical simulations. Aeolian Res. 12, 121–133.

Parteli, E.J., Duran, O., Herrmann, H.J., 2007. Minimal size of a barchan dune. Phys. Rev. E 75 (1), 011301.

Pourteimouri, P., Campmans, G., Wijnberg, K., Hulscher, S., 2023. Modelling the influence of beach building pole heights on aeolian morphology and downwind sediment transport. Geomorphology 108791.

Provoost, S., Jones, M.L.M., Edmondson, S.E., 2011. Changes in landscape and vegetation of coastal dunes in northwest Europe: a review. J. Coast. Conserv. 15, 207–226.

van Puijenbroek, M.E., Limpens, J., de Groot, A.V., Riksen, M.J., Gleichman, M., Slim, P.A., van Dobben, H.F., Berendse, F., 2017a. Embryo dune development drivers: beach morphology, growing season precipitation, and storms. Earth Surf. Process. Landf. 42 (11), 1733–1744.

van Puijenbroek, M.E.B., Nolet, C., de Groot, A.V., Suomalainen, J.M., Riksen, M.J.P.M., Berendse, F., Limpens, J., 2017c. Exploring the contributions of vegetation and dune size to early dune development using unmanned aerial vehicle (UAV) imaging. Biogeosciences 14 (23), 5533–5549.

van Puijenbroek, M.E., Teichmann, C., Meijdam, N., Oliveras, I., Berendse, F., Limpens, J., 2017b. Does salt stress constrain spatial distribution of dune building grasses ammophila arenaria and elytrichia juncea on the beach? Ecol. Evol. 7 (18), 7290–7303.

Pye, K., 1983. Coastal dunes. Progress in Phys. Geogr. 7 (4), 531–557.

Rahn, P.H., 1969. The relationship between natural forested slopes and angles of repose for sand and gravel. Geol. Soc. Am. Bull. 80 (10), 2123–2128.

Ranwell, D.S., Rosalind, B., 1986. Coastal dune management guide. Institute of terrestrial Ecology.

Raupach, M., Gillette, D., Leys, J., 1993. The effect of roughness elements on wind erosion threshold. J. Geophys. Res.: Atmos. 98 (D2), 3023–3029.

Reitz, M.D., Jerolmack, D.J., Ewing, R.C., Martin, R.L., 2010. Barchan-parabolic dune pattern transition from vegetation stability threshold. Geophys. Res. Lett. 37 (19).

Rijkswaterstaat, 2024. Waterinfo. https://waterinfo.rws.nl/ (Accessed: 12 February 2024).

van Rijn, L., Strypsteen, G., 2020. A fully predictive model for aeolian sand transport. Coast. Eng. 156 (March 2020), 1–19.

Riksen, M.J., Goossens, D., Huiskes, H.P., Krol, J., Slim, P.A., 2016. Constructing notches in foredunes: Effect on sediment dynamics in the dune hinterland. Geomorphology 253, 340–352.

Roelvink, D., Costas, S., 2019. Coupling nearshore and aeolian processes: Xbeach and duna process-based models. Environ. Model. Softw. 115, 98–112.

Roelvink, D., Reniers, A., Van Dongeren, A., de Vries, J.V.T., McCall, R., Lescinski, J., 2009. Modelling storm impacts on beaches, dunes and barrier islands. Coast. Eng. 56 (11–12), 1133–1152.

Ruessink, B., Arens, S., Kuipers, M., Donker, J., 2018. Coastal dune dynamics in response to excavated foredune notches. Aeolian Res. 31, 3–17.

Ruessink, G., Sterk, G., Smit, Y., De Winter, W., Hage, P., Donker, J.J., Arens, S.M., 2022. Predicting monthly to multi-annual foredune growth at a narrow beach. Earth Surf. Process. Landf. 47 (7), 1845–1859.

Sauermann, G., Kroy, K., Herrmann, H.J., 2001. Continuum saltation model for sand dunes. Phys. Rev. E 64 (3), 031305.

Sauermann, G., Rognon, P., Poliakov, A., Herrmann, H.J., 2000. The shape of the barchan dunes of southern Morocco. Geomorphology 36 (1–2), 47–62.

de Schipper, M.A., Ludka, B.C., Raubenheimer, B., Luijendijk, A.P., Schlacher, T.A., 2021. Beach nourishment has complex implications for the future of sandy shores. Nat. Rev. Earth Environ. 2 (1), 70–84.

Schwarz, C., Brinkkemper, J., Ruessink, G., 2018. Feedbacks between biotic and abiotic processes governing the development of foredune blowouts: a review. J. Mar. Sci. Eng. 7 (1), 2.

Short, A., Hesp, P., 1982. Wave, beach and dune interactions in southeastern Australia. Mar. Geol. 48 (3), 259–284.

Sigren, J.M., Figlus, J., Armitage, A.R., 2014. Coastal sand dunes and dune vegetation: restoration, erosion, and storm protection. Shore Beach 82 (4), 5–12.

Smyth, T., Jackson, D., Cooper, J., 2011. Computational fluid dynamic modelling of three-dimensional airflow over dune blowouts. J. Coast. Res. 314–318.

Stive, M.J., de Schipper, M.A., Luijendijk, A.P., Aarninkhof, S.G., van Gelder-Maas, C., van Thiel de Vries, J.S., de Vries, S., Henriquez, M., Marx, S., Ranasinghe, R., 2013. A new alternative to saving our beaches from sea-level rise: The sand engine. J. Coast. Res. 29 (5), 1001–1008.

Stockdon, H.F., Holman, R.A., Howd, P.A., Sallenger Jr., A.H., 2006. Empirical parameterization of setup, swash, and runup. Coast. Eng. 53 (7), 573–588.

Strypsteen, G., 2023. The importance of grain-related shear velocity in predicting multi-monthly dune growth. Earth Surf. Process. Landf. 48 (15), 3287–3301.

Strypsteen, G., Bonte, D., Taelman, C., Derijckere, J., Rauwoens, P., 2024. Three years of morphological dune development after planting marram grass on a beach. Earth Surf. Process. Landf..

Strypsteen, G., De Sloover, L., De Wulf, A., Rauwoens, P., 2020. Downwind evolution of aeolian saltation across an artificially constructed coastal berm. Aeolian Res. 47, 100627.

Strypsteen, G., Rauwoens, P., 2023. Aeolian sand transport on a natural beach with shells and moist sand patches. J. Coast. Res. 39, 700–711.

Uphues, C.F., van IJzendoorn, C.O., Hallin, C., Pearson, S.G., van Prooijen, B.C., Miot da Silva, G., de Vries, S., 2022. Coastal aeolian sediment transport in an active bed surface layer: Tracer study and conceptual model. Earth Surf. Process. Landf. 47 (13), 3147–3162.

de Vries, S., Hallin, C., van IJzendoorn, C., van Westen, B., Cohn, N., Strypsteen, G., Skaden, J., Agrawal, N., Garcia Alvarez, M., 2023. AeoLiS. Zenodo, http://dx.doi.org/10.5281/zenodo.10071595.

de Vries, S., de Vries, J.v.T., Van Rijn, L., Arens, S., 2014. Aeolian sediment transport in supply limited situations. Aeolian Res. 12, 75–85.

Wakes, S.J., Maegli, T., Dickinson, K.J., Hilton, M.J., 2010. Numerical modelling of wind flow over a complex topography. Environ. Model. Softw. 25 (2), 237–247.

van der Wal, D., 2004. Beach-dune interactions in nourishment areas along the dutch coast. J. Coast. Res. 20 (1), 317–325.

Walker, I.J., Eamer, J.B., Darke, I.B., 2013. Assessing significant geomorphic changes and effectiveness of dynamic restoration in a coastal dune ecosystem. Geomorphology 199, 192–204.

Walker, I.J., Hilgendorf, Z., Gillies, J.A., Turner, C.M., Furtak-Cole, E., Nikolich, G., 2023. Assessing performance of a "nature-based" foredune restoration project, oceano dunes, california, USA. Earth Surf. Process. Landf. 48 (1), 143–162.

Walker, I.J., Nickling, W.G., 2002. Dynamics of secondary airflow and sediment transport over and in the lee of transverse dunes. Progress in Phys. Geogr. 26 (1), 47–75.

Walker, S.L., Zinnert, J., 2022. Whole plant traits of coastal dune vegetation and implications for interactions with dune dynamics. Ecosphere 13 (5), e4065.

Weng, W., Hunt, J., Carruthers, D., Warren, A., Wiggs, G., Livingstone, I., Castro, I., 1991. Air flow and sand transport over sand-dunes. In: Aeolian Grain Transport: The Erosional Environment. Springer, pp. 1–22.

van Westen, B., Luijendijk, A.P., de Vries, S., Cohn, N., Leijnse, T.W., de Schipper, M.A., 2024. Predicting marine and aeolian contributions to the sand engine's evolution using coupled modelling. Coast. Eng. 188, 104444.

Wijnberg, K., Poppema, D., Mulder, J., van Bergen, J., Campmans, G., Galiforni-Silva, F., Hulscher, S., Pourteimouri, P., 2021. Beach-dune modelling in support of building with nature for an integrated spatial design of urbanized sandy shores. Res. Urban. Ser. 7, 241–260.

Wittebrood, M., de Vries, S., Goessen, P., Aarninkhof, S., 2018. Aeolian sediment transport at a man-made dune system; building with nature at the hondsbossche dunes. Coast. Eng. Proceedings (36), 83.

Zhang, D., Narteau, C., Rozier, O., 2010. Morphodynamics of barchan and transverse dunes using a cellular automaton model. J. Geophys. Res: Earth Surf. 115 (F3).